

To appear in *The Astronomical Journal*

The Redshift Evolution of the Ly α Forest

Tae-Sun Kim¹, Esther M. Hu¹, Lennox L. Cowie¹, and Antoinette Songaila¹

Institute for Astronomy, University of Hawaii, 2680 Woodlawn Dr., Honolulu, HI 96822
 tsk@ifa.hawaii.edu, hu@ifa.hawaii.edu, cowie@ifa.hawaii.edu, acowie@ifa.hawaii.edu

ABSTRACT

We have analyzed the properties of low column density Ly α forest clouds ($12.8 \leq \log N_{\text{HI}} \leq 16.0$) toward 5 QSOs at different redshifts, using high signal-to-noise data from the HIRES spectrograph on the Keck I 10-m telescope. The results are used to study the evolution of these clouds in the interval $2.1 < z < 3.5$. We find: 1) The differential density distribution of forest clouds, $f(N_{\text{HI}})$, fits an empirical power law with a typical slope of $-1.35 \rightarrow -1.55$ for clouds with $N_{\text{HI}} \leq 10^{14.3} \text{ cm}^{-2}$ and changes extremely slowly with redshift over this N_{HI} range. 2) The deviation of $f(N_{\text{HI}})$ from this power-law distribution at higher column densities depends on redshift: for higher redshifts, the departure from a power-law distribution occurs at higher N_{HI} , which means that higher column density clouds rapidly disappear with decreasing redshift. This may be consistent with an invariant shape for the different column density distributions, but with a shift to a lower column density normalization for systems at different redshifts driven by the overall expansion of the universe. 3) The line widths of the forest clouds increase as redshift decreases. 4) The correlation strength of the forest clouds seems to increase as redshift decreases. We discuss these results in terms of the evolution of the IGM comparing the results to models and analytic descriptions of the evolution of structure in the gas.

Subject headings: cosmology: observations — early universe — intergalactic medium — quasars: absorption lines — quasars: individual (0014+813 = S5 0014+81, 0302-003 = Q0302-0019, 0636+680 = S4 0636+68, 1422+231 = B 1422+231, 1623+268 = KP 1623.7+26.8B, 1700+643 = HS 1700+6416)

¹Visiting Astronomer, W. M. Keck Observatory, jointly operated by the California Institute of Technology and the University of California.

1. Introduction

$\text{Ly}\alpha$ forest clouds imprinted in the spectra of high-redshift QSOs provide a unique opportunity to study the evolution of cosmic structure and the distribution of matter in the universe up to $z \sim 5$. The low column density end of the forest is of particular interest, since the number density of forest clouds increases as N_{HI} decreases down to the current observational limit, $N_{\text{HI}} = 3 \times 10^{12} \text{ cm}^{-2}$ (Hu *et al.* 1995, Lu *et al.* 1996, Kirkman & Tytler 1997), and the internal density in these clouds is thought to lie close to the mean baryon density in the intergalactic medium (IGM). Although much observational progress has been made since the advent of the Keck I 10m telescope (which has provided much more sensitive observations of the high- z clouds) and HST (which has accessed the low- z clouds), the evolution of the low column density clouds with redshift has not yet been described. The reason for this is the need for time-consuming high-resolution spectroscopic observations which are essential to detect the forest clouds with H I column densities less than 10^{14} cm^{-2} . It is this topic which we address in the present paper.

Recently, a number of CDM-based numerical simulations have shown that $\text{Ly}\alpha$ forest clouds are a natural consequence of structure formation in the intergalactic gas (Cen *et al.* 1994, Zhang *et al.* 1995, Hernquist *et al.* 1996, Davé *et al.* 1997, Zhang *et al.* 1997). Although the detailed simulation results and input cosmological parameters vary from model to model, there are general trends which may be understood in broad analytic terms (*e.g.*, Hui *et al.* 1996, Bi & Davidsen 1997). In particular, the low column density forest ($N_{\text{HI}} \leq 10^{14} \text{ cm}^{-2}$) forms in regions where the deviations from the mean density are still small, and shocking has yet to occur. (The lowest column density clouds may arise in regions with density lower than the mean density.) The normalization of the column density distribution in this range depends on the ionizing flux, the mean baryon density, and the ionization history of the gas, but the slope of this distribution depends primarily on the amount of power in the fluctuation spectrum at near-Mpc scales, and weakly on the thermal history. Thus the evolution of the distribution function in column density of these clouds is a powerful diagnostic of the formation of structure in the IGM.

Here we use high-resolution, high signal-to-noise spectroscopic data obtained from the Keck I 10m telescope to study the physical properties of lower column density ($N_{\text{HI}} \leq 10^{16} \text{ cm}^{-2}$) forest clouds at $z > 2$ in three different redshift bins. In particular, we address the following three questions: 1) Is there any change in the number density of the lowest column density forest clouds with redshift? 2) Is there any change in the broadening of the clouds with redshift? 3) Is there any significant change in clustering properties with redshift? Sec. 2 describes the observations and data analysis. The observational results are

given in Sec. 3. In Sec. 4 we discuss the observations from the perspective of the numerical simulations and also in a broader context. We summarize our conclusions in Sec. 5.

2. Observations and Data Analysis

The spectra of five QSOs (Q1422+231, Q0014+813, Q0302–003, Q1700+643, and Q1623+268) suitable for studying the Ly α forest at $z > 2$ were selected from an on-going program to study QSO absorption line systems (Songaila 1997). The properties of the clouds seen toward Q0014+813 and Q0302–003 have already been described in Hu *et al.* (1995), but the current analysis includes subsequently obtained data which substantially increased the exposure times. All QSOs were observed at the Keck I 10m telescope with the HIRES spectrograph at a resolution, R , of 36,000 (*cf.* Cowie *et al.* 1995, Hu *et al.* 1995). The properties of the quasars and the exposure times are summarized in Table 1.

The wavelength ranges used for this study were chosen to exclude any higher order hydrogen Lyman absorption lines beyond Ly α and to avoid the proximity effect. Two of the QSOs, Q1422+231 and Q0014+813, have partial Lyman limit systems within the selected wavelength ranges. Ly α forest clouds within $\pm 1000 \text{ km s}^{-1}$ of the partial Lyman limit systems in both QSOs were excluded in order to sample only the “quiet” forest (without possible influence from the partial Lyman limit systems). Table 1 also gives details of the wavelength range and cloud properties.

Voigt profiles, which at these low H I column densities are Gaussians, were fitted to the absorption lines using an automatic line fitting program (Hu *et al.* 1995). Because the lines are formed by a combination of kinematic and thermal broadening, the profile fitting method should not be viewed as a direct model of the underlying reality, but rather as an extremely powerful parameterization of the spectrum which can be compared to similar analyses of simulated model spectra (*e.g.*, Davé *et al.* 1997, Zhang *et al.* 1997) to test the models. The present fitting program selects lines with a central optical depth, $\tau \geq 0.05$, corresponding to an H I column density, $N_{\text{HI}} = 2 \times 10^{12} \text{ cm}^{-2}$ at $b = 30 \text{ km s}^{-1}$ (for thermal broadening the Doppler parameter, $b \equiv \sqrt{2kT/m_p}$, where T is the temperature for a thermally broadened line, m_p is the proton mass, and k is the Boltzmann constant), and then fits the spectrum with an ensemble of profiles characterized by the H I column density, the line width b , and the central redshift z . The program determines a minimal ensemble of lines, since lines can always be fit by a larger number of narrower components. This ambiguity can result in significant differences and may be the primary cause of the differences between Kirkman & Tytler (1997) and Hu *et al.* (1995), who find somewhat different b value distributions at the same redshift. The present analysis is self-consistent in that the five quasars are examined

using the same techniques, and therefore the measured evolution should be robust. However, we discuss in Sec. 3.5 alternative techniques which show the basic results in other forms. Our evolution also matches well to the results of Lu *et al.* (1996) at higher z , despite the possible differences in analysis techniques.

All QSO spectra, except for that of Q1623+268, have S/N of $\gtrsim 40$ per resolution element, and Q1422+231 has S/N of near 140 per resolution element. In the case of Q1623+268 the low blue sensitivity of the HIRES CCD at wavelengths shorter than 4000Å dropped the S/N to ~ 20 over the wavelengths studied. To construct a homogeneous data set, we only used the lines with $N_{\text{HI}} \geq 6.3 \times 10^{12} \text{ cm}^{-2}$ from the 4 other QSO spectra. This also restricts us to the column density range where any incompleteness corrections are small (Hu *et al.* 1995). Although it is hard to quantify the saturation of the lines because of the spread in b values, we begin to see these effects at about $N_{\text{HI}} \geq 1.5 \times 10^{14} \text{ cm}^{-2}$ for $b = 30 \text{ km s}^{-1}$ if we define a saturated line as a line with a residual flux $r_{\nu} = \exp(-\tau_{\nu})$ less than 0.025. As long as the lines did not show any severe departures from a Voigt profile, all saturated lines were fitted with a single component.

All possible metal-line candidates were examined. Unlike the case for the $z < 1$ forest, it is not straightforward to distinguish metal lines in the forest at $z > 2$ due to the higher number density of forest clouds. Keeping in mind that most metal lines have lower b values ($< 15 \text{ km s}^{-1}$) than those of forest clouds when fitted as H I lines (Hu *et al.* 1995), it is rather easy to recognize C IV ($\lambda\lambda 1548, 1550$) and Si IV ($\lambda\lambda 1393, 1402$). With the exception of the spectrum of Q1700+643, most C IV and Si IV doublets commonly associated with higher column density forest clouds either lie outside the wavelength regions under consideration or were not found. Metal lines from the lower redshift metal line systems were also examined and excluded. However, broad metal lines such as Si III ($\lambda 1206$) are hard to identify correctly in the forest and may not be completely removed. In any case, the fraction of metal lines in the forest will not be higher than 5%, and the number counts are dominated by Poisson noise.

For Q1700+643, which is known to have at least 10 low-redshift metal line systems (Reimers & Vogel 1993, Vogel & Reimers 1995, Rodriguez-Pascual *et al.* 1995), a thorough search was made for metal lines and these were removed. However, there are 9 unidentified lines with $b \leq 20 \text{ km s}^{-1}$ in the Q1700+643 forest compared to 1 line in the Q1623+269 forest over the column density range, $N_{\text{HI}} = 10^{13.1} - 10^{15} \text{ cm}^{-2}$. We included these unidentified lines in our list of Ly α forest clouds; however, they are most likely unidentified metal lines from the metal line systems towards Q1700+643. Since the number of unidentified narrow lines is at most 11% of the $b \leq 20 \text{ km s}^{-1}$ systems, the inclusion or exclusion of these lines does not affect the conclusions reached in this analysis.

We grouped the 5 QSOs into three different redshift bins (Table 1), with central values of $< z > = 2.31$ (Q1623+268, Q1700+643), $< z > = 2.85$ (Q0014+813, Q0302–003), and $< z > = 3.35$ (Q1422+231).

3. Results

3.1. Differential Density Distribution Function

The differential density distribution function (hereafter DDF or $f(N_{\text{HI}})$) is defined as the number of absorbing systems per unit redshift path per unit column density as a function of N_{HI} . The redshift path $X(z)$ is defined by $X(z) \equiv \frac{1}{2}[(1+z)^2 - 1]$ for $q_0 = 0$ or by $X(z) \equiv \frac{2}{3}[(1+z)^{3/2} - 1]$ for $q_0 = 0.5$.

Fig. 1 shows the DDF, without any correction for blending or incompleteness, at different redshifts. The stars represent $< z > = 3.35$, the triangles $< z > = 2.85$, and the diamonds $< z > = 2.31$. The open circles are for $< z > = 3.70$ from Lu *et al.* 1996. The solid line represents the single power-law fit, $f(N_{\text{HI}}) = 4.9 \times 10^7 N_{\text{HI}}^{-1.46}$, taken from Hu *et al.* (1995) for their data at $z \sim 2.85$. The dotted line represents the single power-law fit for $z \sim 3.7$ Ly α forest clouds, $f(N_{\text{HI}}) \propto N_{\text{HI}}^{-1.55}$ estimated from Fig. 6 of Lu *et al.* (1996), and matched to the same $f(N_{\text{HI}})$ at $\log N_{\text{HI}} = 14.15$. This slope of -1.55 at $< z > = 3.7$ was obtained from the fit to the column density range $N_{\text{HI}} = 10^{12.6-16.0} \text{ cm}^{-2}$ with the incompleteness correction applied. However, over the column density range $N_{\text{HI}} = 10^{12.3-14.5} \text{ cm}^{-2}$, Lu *et al.* (1996) found a slope of -1.46 , which matches the value found by Hu *et al.* (1995) and Kirkman & Tytler (1997) at redshifts near 3.

There are two notable features of Fig. 1. First, the four DDFs roughly follow a single power-law, $f(N_{\text{HI}}) \propto N_{\text{HI}}^{-\beta}$, with $\beta \sim 1.4$ over the column density range $N_{\text{HI}} = 10^{12.8} - 10^{14.3} \text{ cm}^{-2}$. The DDFs do not show any sign of flattening in this range with the possible exception of the $< z > = 3.70$ DDF at lower H I column density. However, the lowest N_{HI} points for Lu *et al.* have higher levels of incompleteness correction and this result is correspondingly uncertain. Earlier results claimed that there was a flattening in the DDF at $N_{\text{HI}} \leq 10^{13.8} \text{ cm}^{-2}$ (Petitjean *et al.* 1993). However, this flattening is mainly caused by blending in low resolution data and was not confirmed from the Keck HIRES data down to $N_{\text{HI}} \sim 10^{12.5} \text{ cm}^{-2}$ at $z \sim 2.85$ (Hu *et al.* 1995). We now see this result holds over the $z = 2 - 4$ redshift range, and also provides a good description of the Lu *et al.* (1996) results.

Second, at the higher column density end, $N_{\text{HI}} \geq 10^{14.3} \text{ cm}^{-2}$, the DDFs for the redshift intervals differ substantially. Except at the highest redshift there is a strong lack of forest clouds at high column densities compared with the number expected from the power-law

distribution at $N_{\text{HI}} \leq 10^{14.3} \text{ cm}^{-2}$ (see Petitjean *et al.* 1993). This deficiency cannot be a result of misestimates in the column density owing to saturation effects since the total number of clouds is deficient relative to the extrapolated power law (Hu *et al.* 1995). The $\langle z \rangle = 3.70$ data of Lu *et al.* (1996) show only a slight steepening at the higher column densities, but by $\langle z \rangle = 3.35$ forest clouds deviate from the power-law at $N_{\text{HI}} \sim 10^{14.8} \text{ cm}^{-2}$, while those at $\langle z \rangle = 2.85$ and $\langle z \rangle = 2.31$ deviate from the power-law at $N_{\text{HI}} \sim 10^{14.3} \text{ cm}^{-2}$. Furthermore, the degree of deficiency in cloud numbers compared to predictions from the single power-law fit also depends on redshift. The $\langle z \rangle = 2.31$ clouds deviate from the power-law more rapidly than the $\langle z \rangle = 2.85$ clouds and the $\langle z \rangle = 3.35$ clouds. There are no clouds with $N_{\text{HI}} \geq 10^{15.2} \text{ cm}^{-2}$ at $\langle z \rangle = 2.31$. The redshift path for $\langle z \rangle = 2.31$ is 1.5 times larger than that for $\langle z \rangle = 3.35$, so this deficiency of higher column density clouds in the lower redshift range cannot be an observational selection effect. Thus the break in the density distribution function appears to be strengthening and migrating to lower column densities as the redshift decreases.

3.2. Number density of Ly α forest clouds with redshift

The evolution in Ly α forest clouds with redshift has traditionally been explored by looking at the number density of clouds in a given column density range as a function of redshift. The number density per unit redshift per line of sight is expressed as $N(z) = N_{\text{o}}(1+z)^{\gamma}$, where $N_{\text{o}} = \Phi_{\text{o}}\pi R_{\text{o}}^2 c H_{\text{o}}^{-1}$. The parameter Φ_{o} is the local comoving number density of forest clouds, πR_{o}^2 is the local cross section of a cloud, and c and H_{o} are the speed of light and the Hubble constant, respectively. This yields $\gamma = 1$ for $q_{\text{o}} = 0$ and $\gamma = 0.5$ for $q_{\text{o}} = 0.5$ for non-evolving clouds. However, it is clear from the evolution of the shape in the DDF that the measured γ will be a function of the chosen column density interval and of redshift, except at low column density. This greatly complicates this type of analysis, and comparisons between individual studies based on this method are difficult.

HST observations show a value for $\gamma = 0.48 \pm 0.62$ at $z < 1$, which is consistent with no evolution (Bahcall *et al.* 1993). However at higher redshift, $z > 2$, a rather wide range of γ values has been obtained, from $\gamma = 2.75 \pm 0.29$ (Lu *et al.* 1991; indicating strong evolution) to $\gamma = 2.36 \pm 0.40$ (Bajtlik *et al.* 1988) to $\gamma = 1.89 \pm 0.28$ (Bechtold 1994; indicating weak evolution). An inflection in $N(z)$ from the redshift-limited samples has also been pointed out, suggesting that γ is different in different redshift ranges (Lu *et al.* 1991, Bechtold 1994, Impey *et al.* 1996). These results have been used to suggest that Ly α forest clouds do not consist of a single population and that a different population becomes dominant at different redshifts (Boksenberg 1995).

Keeping in mind that $N(z)$ is sensitive to the adopted threshold N_{HI} (a reflection of the form of departure from the single-power law distribution at $N_{\text{HI}} \geq 10^{14.3} \text{ cm}^{-2}$), we fitted the data to a conventional single power-law form, for lines with $N_{\text{HI}} = 10^{13.77} - 10^{16} \text{ cm}^{-2}$. This corresponds roughly to the conventional equivalent width threshold, $W = 0.32\text{\AA}$, and enables us to compare the present data directly with the results of Bechtold (1994) and Impey *et al.* (1996). Fig. 2 shows $N(z)$ as a function of redshift. The vertical bars indicate the 1σ errors and the horizontal bars indicate the bin sizes for the individual QSOs. No incompleteness correction was made; over this column density range, it is rather small (less than 10%) and within the 1σ error bars. The filled circles show the Keck HIRES data for our 5 QSOs and the open circle that of Lu *et al.* (1996). The open triangles show the Keck HIRES data only for the lower column density systems with $N_{\text{HI}} = 10^{13.1} - 10^{14.0} \text{ cm}^{-2}$. The diamonds are taken from Impey *et al.* (1996) for HST observations of PG1222+228 and PG1634+706 and the open squares are taken from Bahcall *et al.* (1993) for HST observations of PKS 0044+03, 3C 273, and 3C 351. The region shown by dashed lines represents the measurement of Bechtold (1994), which is a factor of 2 lower than our observations. This is probably explained by the 7 times higher resolution in our data, which is capable of deblending neighboring lines which, especially at higher redshifts, can be a serious problem. Our data yield a factor of 2.3 more lines at $z \sim 3.2$ and a factor of 1.3 more lines at $z \sim 2.4$ than found by Bechtold (1994), consistent with this interpretation of the discrepancy.

The maximum likelihood method (Murdoch *et al.* 1986) was used to derive the best estimated γ values for the above data. The best fit using only the present Keck data in our study at $3.5 > z > 2$ (the dotted line) yields $\gamma = 2.78 \pm 0.71$, consistent with $\gamma = 1.89 \pm 0.28$ by Bechtold (1994) within a 2σ error. The best fit for N_{o} is $N_{\text{o}} = 3.12$. The uncertainty in N_{o} was not calculated since it is strongly correlated with γ . At lower redshifts, $z < 1.5$, line blending becomes less of a problem than for $z > 2$ systems, since the number density of clouds is smaller, and the HST counts should be directly relatable to the Keck counts. When our data is combined with the HST observations (Bahcall *et al.* 1993, Impey *et al.* 1996), the best fit for $0 < z < 3.6$ yields $\gamma = 2.15 \pm 0.21$ and $N_{\text{o}} = 6.89$ (the solid line). Because there are only 15 forest clouds at $z < 1$, the maximum likelihood method puts high emphasis on the numerous and more densely covered (in redshift space) high-redshift observations, resulting in a higher γ than that obtained with a least-squares fit, $\gamma = 1.74 \pm 0.14$. The γ value driven by the maximum likelihood method is also higher than the one ($\gamma = 0.48$) estimated from the $z < 1$ data (Bahcall *et al.* 1993) or the one ($\gamma = 1.26$) from the $0 < z < 4$ data obtained by Bechtold (1994). The latter result is a consequence of Bechtold's lower number counts. The value of N_{o} is also correspondingly smaller (by a factor of 3) than that obtained by Bahcall *et al.* (1993) ($N_{\text{o}} \sim 19.0$) because of the higher γ . The present high γ values show that the number of higher column density clouds at $z > 1$ declines rapidly with

decreasing redshift. When the $< z > = 3.7$ systems are included, the value of γ for $0 < z < 4$ is 2.41 ± 0.18 . However, considering the different treatment applied to the different data sets, this estimated value should be taken with caution.

When we count only Ly α forest clouds in the column density range of $N_{\text{HI}} = 10^{13.1} - 10^{14} \text{ cm}^{-2}$, where the DDF is well-fitted by a common power-law for systems at all redshifts, we obtain a best fit (the long-dashed line) $\gamma = 1.29 \pm 0.45$ and $N_0 = 39.44$ for the $z > 2$ systems. This γ value is consistent within the errors with a non-evolving model ($\gamma = 1$), as we would expect from our discussion of the DDF. Although the lack of lower column density forest clouds at $z < 1$ prevents extrapolation of these fitted values, it appears that the DDF and $N(z)$ of these lower column density clouds do not evolve with redshift at $z > 2$.

3.3. The change in b value with redshift

The line widths are characterized by the Doppler parameter, b , in the profile fitting. Figs. 3a–c show $b - \log N_{\text{HI}}$ diagrams at average redshifts $< z > = 2.31$, $< z > = 2.85$, and $< z > = 3.35$. As is shown in the diagrams, most lines with $b < 15 \text{ km s}^{-1}$ are metal lines. There seems to be a reasonably well-defined minimum b value (b_c) over the N_{HI} range at each redshift when the metal lines are discarded (see also Hu *et al.* 1995 and Lu *et al.* 1996, though this result is questioned by Kirkman & Tytler 1997), implying that the b value distribution is truncated at the low end. (Note the increase in the number of lines with $N_{\text{HI}} \geq 10^{14} \text{ cm}^{-2}$ with increasing redshift.) Also the number of clouds with $b \leq 20 \text{ km s}^{-1}$ (the b_c value at $z \sim 2.85$ shown as a dashed line) decreases as the redshift decreases, suggesting that b_c is increasing with decreasing redshift (see also Lu *et al.* 1996).

In order to quantify the changes in b_c and determine the corrections to the DDF for line blending and incompleteness and the profile fitting methodology, we followed the procedures of Hu *et al.* (1995). We generated artificial spectra and fitted them in the same way as we treat the observed data. We assumed the slope in the DDF to be 1.5 in order to compare to the $< z > = 2.85$ clouds (Hu *et al.* 1995), and used a random distribution of clouds at a given redshift range. For b values, we used a Gaussian distribution, but truncated it at a value lower than the cut-off value, b_c , at each redshift. The fitted artificial counts are then compared to the input counts to determine the changes caused by blending. This incompleteness correction at $< z > = 2.31$ and at $< z > = 3.35$ as a function of column density is given in Table 2, while the incompleteness correction at $< z > = 2.85$ is taken from Hu *et al.* (1995). Fig. 4 shows the incompleteness corrected differential density distribution functions. Since the line density is larger at higher redshift, the incompleteness correction at $< z > = 3.35$ is slightly more sensitive to the assumed β and the fitted N_{HI} range. Assuming $\beta = 1.5$, the

resulting β is ~ 1.58 for $N_{\text{HI}} = 10^{12.8} - 10^{14.3} \text{ cm}^{-2}$ and ~ 1.53 for $N_{\text{HI}} = 10^{12.8} - 10^{14.8} \text{ cm}^{-2}$. The incompleteness correction at $< z > = 2.31$ is not as sensitive to the assumed β as the $< z > = 3.35$ clouds. Here, the observed low β of 1.28 results in a low β of 1.35 after the incompleteness correction. For $< z > = 3.35$, $f(N_{\text{HI}}) = 3.3 \times 10^9 N_{\text{HI}}^{-1.59 \pm 0.13}$ (2σ error). For $< z > = 2.31$, $f(N_{\text{HI}}) = 1.5 \times 10^6 N_{\text{HI}}^{-1.35 \pm 0.03}$ (2σ error). We note that using only the two $< z > = 2.85$ systems, Q0014+813 and Q0302-003, gives an incompleteness corrected DDF having a best fit of $f(N_{\text{HI}}) = 5.7 \times 10^6 N_{\text{HI}}^{-1.39 \pm 0.26}$ (2σ error) over the column density range $N_{\text{HI}} = 10^{12.8} - 10^{14.3} \text{ cm}^{-2}$. This is slightly shallower than the -1.46 slope obtained by Hu *et al.* (1995) with two additional quasars included for this redshift interval. Although there might be some deviation at the lower N_{HI} end in the distribution function (where the incompleteness correction is very uncertain), the three DDFs show an excellent match at $N_{\text{HI}} = 10^{13.7} - 10^{14.3} \text{ cm}^{-2}$ where the incompleteness correction is not high. Within the 2σ errors and the systematic errors in the profile fitting methodology, these β values could be treated as consistent with the $< z > = 2.85$ forest clouds with $\beta = 1.46 \pm 0.07$, but overall there does seem to be evidence that there is a very weak flattening of β with decreasing redshift. However, we conclude again that unlike the case for high column density clouds ($N_{\text{HI}} \geq 10^{14.3} \text{ cm}^{-2}$), the DDF does not change rapidly with redshift, within the observational and simulated errors for $N_{\text{HI}} \leq 10^{14.3} \text{ cm}^{-2}$.

The procedure of incompleteness correction also produces an estimated b_c value. With an assumed β , three parameters of a truncated Gaussian b distribution are varied until a satisfactory match to the observations is obtained: median(b), $1\sigma(b)$, and b_c . Fig. 5 shows the averaged simulated b distribution (the solid lines) with the observed b distribution (the dotted line) at $< z > = 2.31$ and $< z > = 3.35$. With the large number of lines at $< z > = 3.35$, the cut-off b value, b_c , is rather straightforward to determine: $b_c = 17 \text{ km s}^{-1}$ (or $T_c = 1.8 \times 10^4 \text{ K}$, if we assume a thermal broadening), $1\sigma = 8 \text{ km s}^{-1}$, and median(b) = 26 km s^{-1} . No perfect fit was found for the $< z > = 2.31$ forest clouds. With $b_c = 22 \text{ km s}^{-1}$, more than 50% of the simulations generated too many lines with $b = 19 - 22 \text{ km s}^{-1}$ when compared to the observations. Assuming that most narrow lines are metal lines (90% of the unidentified lines with $b \leq 20 \text{ km s}^{-1}$ are from the Q1700+643 with 10 metal line systems), we took the best fit value for the observation namely at $b \geq 20 \text{ km s}^{-1}$: $b_c = 24 \text{ km s}^{-1}$ (or $T_c = 3.5 \times 10^4 \text{ K}$, if thermally broadened), $1\sigma = 12 \text{ km s}^{-1}$, and median(b) = 30 km s^{-1} .

These results show that there is an increase in the b_c value as redshift decreases which is also consistent with $b_c = 15 \text{ km s}^{-1}$ determined at $z = 3.4 \rightarrow 4.0$ by Lu *et al.* (1996). These results are shown in Fig. 6a. Fig. 6b shows the median b values for each QSO. The solid line is for $N_{\text{HI}} = 10^{13.8} - 10^{16} \text{ cm}^{-2}$ and the dotted line is for $N_{\text{HI}} = 10^{13.1} - 10^{14} \text{ cm}^{-2}$. Table 3 lists the median b values for each QSO. This rising trend in both b_c and the median b values

suggests that the internal temperatures and/or the level of kinematic broadening are rising with decreasing redshift, as we shall discuss further in Sec. 4.

3.4. Correlation Function

The simplest way of testing inhomogeneity in the space distribution of Ly α forest clouds is to calculate the two-point velocity correlation function, ξ . Among different ways of calculating ξ , the most widely used method is comparison between the observed number of pairs (N_{obs}) and the expected number of pairs (N_{exp}) from the random distribution in a given velocity bin (Δv); $\xi(\Delta v) = N_{obs}(\Delta v)/N_{exp}(\Delta v) - 1$, where $\Delta v = c(z_2 - z_1)/[1 + (z_2 + z_1)/2]$ and z_1 and z_2 are the redshifts of two lines. Although this formula is correct only in the limit of an ideal large sample and is sensitive to the bin size, general information on clustering can be obtained by this method.

Searches for clustering in Ly α forest clouds have been a function of resolution, S/N, bin size, and possibly line of sight, and there have been rather mixed results to date. Sargent *et al.* (1980) and Rauch *et al.* (1992) find no positive correlation at any velocity scale. On the other hand, Cristiani *et al.* (1995), and Hu *et al.* (1995) show an anti-correlation at $\Delta v = 600 - 900$ km s $^{-1}$ as well as a positive correlation at $\Delta v < 200$ km s $^{-1}$. While this anti-correlation is also claimed to exist by Meiksin & Bouchet (1995), Cristiani *et al.* (1997) failed to confirm the reality of anti-correlation from a larger data set, but did confirm the positive correlation at $\Delta v < 300$ km s $^{-1}$.

The correlation functions at the three redshifts were calculated relative to the average of 500 simulations with a 50 km s $^{-1}$ velocity bin for each QSO. We used lines with $N_{HI} \leq 10^{16}$ cm $^{-2}$ for this calculation, although there are few lines with $N_{HI} \geq 10^{15}$ cm $^{-2}$.

Fig. 7a shows the averaged correlation function as a function of redshift for systems with column densities above a threshold value, $N_{HI,th}$, such that $\log N_{HI,th} > 13.8$. The dotted lines are the 1σ Poisson errors. While there is suggestion of a positive correlation for $< z > = 2.31$ at $\Delta v < 300$ km s $^{-1}$ (a 2.8σ significance at $\Delta v = 75$ km s $^{-1}$), there is no significant correlation strength at $< z > = 2.85$. This is in disagreement with what was found by Hu *et al.* (1995) with an overlapping HIRES data set. We will discuss this point later. At $< z > = 3.35$, a positive correlation may exist at a 2.54σ significance at $\Delta v = 75$ km s $^{-1}$. Given the large time gap between $z = 3.35$ and the present day, the interpretation of the correlation functions with redshift is ambiguous. However, the clustering should evolve strongly with redshift at $z = 2.31 \rightarrow z = 0$ if Ly α forest clouds follow more or less the highly structured present day galaxies (Hernquist *et al.* 1996, but see Morris *et al.* 1993). Fig. 7b

shows the correlation strength at $\Delta v = 75 \text{ km s}^{-1}$ as a function of threshold column density $N_{\text{HI,th}}$, for three redshift bins. As Cristiani *et al.* (1997) pointed out, at $< z > = 2.31$ and $< z > = 3.35$, the correlation strengths seem to increase as $N_{\text{HI,th}}$ increases. At $< z > = 2.85$, this trend does not hold tightly. However, as Fig. 7c shows, when averaged for all redshifts, the correlation strength does increase as $N_{\text{HI,th}}$ increases.

3.5. Alternative Descriptions

Figs. 8a and 8b show two alternative descriptions of the data (*e.g.*, Croft *et al.* 1997). Fig. 8a shows the normalized cumulative distribution of the flux decrements $D \equiv 1 - e^{\tau}$ for the five quasars computed in the wavelength ranges specified in Table 1. The distributions agree well with similar observations by Rauch *et al.* (1996) and also with model predictions for a suitable choice of $\Omega_b h^2 T^{-0.7}/J$ (*e.g.*, Rauch *et al.* 1996, Croft *et al.* 1997). Fig. 8b shows the number of times the spectrum crosses down across a given decrement per unit X . In the absence of blending and given the invariance of the *DDF*, narrower b values will result in a higher number of crossings. Thus, the increased rate of crossings seen at higher z for the larger flux decrements is an alternative method of seeing that the lower z clouds are broader. At small flux decrements blending becomes important, and because this effect is larger at higher z , this reverses the sign of the effect.

4. Discussion

4.1. The column density distribution function

The number density per unit redshift path X per unit N_{HI} (the density distribution function) as a function of redshift depends on the history of the UV ionizing background, the mean baryon density, and the underlying cosmology, and only detailed numerical simulations can give complete descriptions of these combined effects to compare with the observations.

Simulations by Mücke *et al.* (1996) show broad consistency with the present data, with high column density clouds ($N_{\text{HI}} > 10^{14} \text{ cm}^{-2}$) evolving as $16.8(1+z)^{0.8} + 0.687(1+z)^{2.5}$ while low column density clouds ($N_{\text{HI}} < 10^{13} \text{ cm}^{-2}$) evolve only as $(1+z)^{0.7}$. However, Fig. 9 shows that the observed rise for the high column density ($10^{14} < N_{\text{HI}} < 10^{16} \text{ cm}^{-2}$) clouds is somewhat steeper than this prediction. Lu *et al.*'s results at $< z > = 3.7$ are also shown, and are consistent with the fit obtained for $< z > = 2.31 \rightarrow 3.35$. The more sophisticated treatment of Davé *et al.* (1997), using Voigt profile fitting to artificial spectra generated from their SPH simulations, shows a *DDF* that drops by a factor of $1.5 - 2$ for $z = 3 \rightarrow 2$ at

$N_{\text{HI}} \geq 10^{13.2} \text{ cm}^{-2}$, while at $N_{\text{HI}} \leq 10^{13.2} \text{ cm}^{-2}$, the number of clouds increases by a factor of 2 for $z = 3 \rightarrow 2$. These features in the predicted DDF do not match the observations, which show a larger number of clouds at $z \sim 3$ compared to those at $z \sim 2$ only for those clouds with $N_{\text{HI}} \geq 10^{14.3} \text{ cm}^{-2}$, but this may be due at least in part to the profile fitting methodology. Both Davé *et al.* (1997) and Weinberg *et al.* (1997) find relatively steep profiles with $\beta = 1.7$ as do Mückel *et al.* (1996). However, Zhang *et al.*'s (1997) similar analysis of their hierarchical grid code simulation shows a remarkably good agreement both with the overall shape of the DDF at $z = 2.9$ ($\beta \approx 1.5$), and with the redshift evolution seen in the present data, finding γ for $W \geq 0.32 \text{ \AA}$ selected clouds of 2.95 ± 0.4 for $z = 1.5 \rightarrow 3.5$ and 0.24 ± 0.03 for $z < 1.5$, which is in good agreement with Fig. 2 and the discussion of Sec. 3.3. It is unclear whether the differences between Davé *et al.* and Zhang *et al.* (which are also reflected in the b value distributions discussed below) are a consequence of details of the codes, choice of parameters (particularly the fluctuation spectra), or details of the profile fitting analysis, but the results do suggest that within the tunability and uncertainty in the current models that it is possible to obtain remarkably good agreement with the data.

The analytic models of Hui *et al.* (1996) give considerable insight into the origin and invariance of the slope. At these low column densities the temperature is set by the balance between adiabatic expansion and ionization heating, and may be described by a polytropic equation of state $T \sim \rho^{\gamma-1}$, where $(\gamma-1)$ lies between 0 and 0.62, depending on the ionization history. The slope of the DDF is then given by

$$\beta = 1 + \left[\frac{0.96 - 2(\sigma_o - 1)}{1.68 - 0.7(\gamma - 1)} \right] \quad (1)$$

where σ_o is the RMS density fluctuation at scales close to the Jeans length (Hui *et al.* 1996). For the observed β values and for the possible range of γ values, σ_o is extremely tightly constrained to a value of 1.15, with a plausible range of only ± 0.1 . The flattening of the β value with decreasing redshift would require γ to be closer to isothermal at the lower redshifts, which is counter to the expected evolutionary trend. This may, however, be related to reionization of the He if this occurs around $z = 3$ as has been suggested based on the evolution of metal line ratios (Songaila & Cowie 1996).

The deviation from the power law at the high column density end would then correspond to the overdensity at which shocking occurs (*e.g.*, Mückel *et al.* 1997), which is approximately ten times the mean density at the given redshift. If the column density at which the deviation occurs does correspond to the shocking overdensity then we expect it to scale roughly as $(1+z)^6 T^{-0.7} J^{-1}$, where T is the temperature and J the ionizing flux. If the ionizing flux is roughly constant over the redshift range (Haardt & Madau 1996) and the temperature changes only slowly with redshift as in the limit of early ionization (Hui & Gnedin 1996), N_{dev}

would drop by 0.8 in the log between $z = 3.5$ and $z = 2.3$, which is somewhat larger than the observed drop from $\log N_{\text{HI}} = 14.8$ to 14.3. This suggests that J is falling with decreasing redshift or that the temperature is rising. The latter effect could again be associated with helium reionization.

4.2. The evolution of b values

If the Ly α forest lines were intergalactic clouds in thermal equilibrium with the metagalactic UV ionizing background without any other energy source, the line width of the clouds (or the Doppler parameter, b) would measure the temperature of the clouds. However, within the structure evolution models the low column density forest clouds ($N_{\text{HI}} < 10^{14} \text{ cm}^{-2}$) are primarily kinematically rather than thermally broadened. Two important observations may be taken from the Keck HIRES data. First, there seems to be a rough lower cut-off b value (b_c) which increases with decreasing redshift. Most forest clouds have a b value similar to or greater than b_c , whereas most lines with $b < b_c$ are identified as metal lines. Hu *et al.* (1995) interpreted b_c as the minimum b value in a single region, with most Ly α clouds being a blend of several components. Secondly, taking the median b as 34 km s^{-1} and $b_c = 20 \text{ km s}^{-1}$ suggests that the additional broadening due to the multiple components is very similar to b_c (Cowie *et al.* 1995). The increase in the b values with decreasing redshift is likely to be a reflection of the ongoing increase in structure.

The numerical simulations of Davé *et al.* (1997) give higher b values than are observed at $z \sim 3$, while the simulations of Zhang *et al.* (1997) provide fairly good agreement with the observations. (Both are broader than the distribution of Kirkman & Tytler 1997.) This is a similar effect to that seen in the DDF, and may indicate some fundamental difference between the SPH and grid simulations. There is as yet no discussion of the evolution of the b value distribution, though the overall increase in the width with redshift is in the sense expected from the models.

For the higher column density clouds which have entered the shocked regime the widths will reflect primarily the thermal broadening, and the minimum widths may then correspond to minimum temperatures (*e.g.*, Haehnelt *et al.* 1996). However, even for these clouds the evolution of internal temperatures governed solely by ionization equilibrium is insufficient to provide an explanation of the evolution of b_c . Songaila & Cowie (1996) show that Si IV/C IV in the forest clouds at $2.1 < z < 3.8$ is well described by a hypothetical He II ionization front at $z \sim 3.1$, with Si/C = 3 times the solar value, since the ratio of Si IV/C IV is sensitive at the high energy end in the assumed metagalactic UV flux. If there is a He II ionization front at $z \sim 3.1$, this ionization causes a change in the metagalactic UV flux, and thus the

b value in the forest clouds. We tested this effect using a broken power law for the UV flux, following the same procedure as Giallongo & Petitjean (1994), where the amount of He II ionization is characterized by a parameter B , which is the relative flux at 4 ryd and 4.5 ryd. Assuming the flux at the Lyman Limit (1 ryd) of $J_o = 10^{-21}$ erg cm $^{-2}$ s $^{-1}$ Hz $^{-1}$ and a single power-law for the UV energy spectra with $\alpha = 1.5$ ($J_\nu \propto \nu^{-\alpha}$) (Cooke *et al.* 1997), we ran the photoionization model of Ferland (1993). The calculation was made for clouds with $N_{\text{HI}} = 10^{14.5}$ cm $^{-2}$ and we used a 10^{-2} solar metallicity with Si/C = 3. Fig. 10 shows the model calculations with different ionization parameters, $\Gamma \sim J_o/n_e$. The long-dashed line is for $B = 1$ (no He II ionization); the dotted line, the dashed line, the dot-dashed line, and the dot-dot-dashed line are for $B = 10$, $B = 100$, $B = 1000$, and $B = 10000$, respectively. Songaila & Cowie (1996) found a satisfactory result for the Si and C ratios with $B \geq 100$ for $z > 3.1$ and $B = 1 - 10$ for $z < 3.1$. At $< z > = 2.85$, the model-calculated b for the hydrogen clouds is well-matched with the $B = 1 - 10$ spectra at $\Gamma = 10^{-2} - 10^{-1.5}$ and at $< z > = 3.35$ and 3.7, the b_c values are also in the regime of the photoionization prediction with $B = 100$. However, at $< z > = 2.31$, the b_c value is too high for the photoionization model to obtain (for either $b_c = 22$ km s $^{-1}$ or $b_c = 24$ km s $^{-1}$). Thus evolution in b_c cannot be fully accounted for by evolution of an equilibrium photoionization temperature. A hypothetical He II ionization at $z \sim 3.1$ can explain the evolution of b_c values at $z > 2.5$, but fails to explain the b_c of 24 km s $^{-1}$ at $< z > = 2.31$. The lower redshift clouds clearly require a higher dynamical energy input than the high redshift clouds. This may reflect a higher level of overall turbulence at the lower redshifts, as evidenced by the increase in the median b values.

4.3. Ly α forest contribution to Ω_b

One of the most important cosmological parameters is the ratio of the baryon density to the critical density in the universe, Ω_b , which can be directly compared with the predictions of big bang nucleosynthesis. At $z = 2 - 4$ the intergalactic gas may still comprise most of the baryons in the universe and thus the QSO absorption line systems can provide a direct measurement of Ω_b .

Numerical simulations of the Lyman forest have generally favored a high $\Omega_b h^2$ ($\gtrsim 0.0125$) (*e.g.*, Rauch *et al.* 1996, Weinberg *et al.* 1997), though a more direct study of the He II opacity suggests a lower Ω_b (Hogan *et al.* 1997). All of these methods are dependent on assumptions about the evolution of the shape and normalization of the ionizing field (as well as its fluctuations), which determine the cloud internal temperatures and the conversion from neutral to total hydrogen. It is also possible that the current simulations may not be

adequately dealing with the structure on the smaller scales (Croft *et al.* 1997), which again could result in uncertainties in the relative normalization of the hydrogen optical depth relative to Ω_b . Here we shall adopt a more empirical approach to determining the evolution of Ω_b from the observations.

The contribution to $\Omega_b(\text{H I})$ from the Ly α forest can be directly obtained by integrating through the DDF. In units of the local critical density ρ_c , the mass density of H I in the Ly α forest is

$$\Omega_b(\text{HI}) = \frac{H_o}{c} \frac{\mu m_H}{\rho_c} \int_{N_{\text{min}}}^{N_{\text{max}}} N_{\text{HI}} f(N_{\text{HI}}) dN_{\text{HI}}, \quad (2)$$

(*e.g.*, Lanzetta *et al.* 1991). The parameter m_H is the hydrogen mass, c is the speed of light, H_o is the Hubble constant, and $N_{\text{min}} - N_{\text{max}}$ is the H I range of the forest clouds. The parameter μ is the mean mass per proton mass and is taken as 1.3.

Because the DDF is everywhere shallower than a -2 power-law slope, $\Omega_b(\text{H I})$ is always dominated by the highest column density clouds. In Table 4 we summarize $\Omega_b(\text{H I})$ from clouds below $2 \times 10^{14} \text{ cm}^{-2}$, which is always below the break, and also the total $\Omega_b(\text{H I})$ for $N_{\text{HI}} < 4 \times 10^{15} \text{ cm}^{-2}$. In the lower N_{HI} range which is below the break, $\Omega_b(\text{H I})$ is roughly constant at $6 \times 10^{-8} h^{-1}$ over the redshift range, reflecting the rough invariance of the DDF, while in the higher column densities $\Omega_b(\text{H I})$ drops from $2.5 \times 10^{-7} h^{-1}$ at $z = 3.7$ to $1.1 \times 10^{-7} h^{-1}$ at $z = 2.31$, reflecting the decreasing number of clouds.

In order to translate $\Omega_b(\text{H I})$ to Ω_b we need to know the appropriately weighted ionization fraction $F = \text{H I}/\text{H}$ in the clouds. At the high column density end ($N_{\text{HI}} \gtrsim 10^{15} \text{ cm}^{-2}$) the ionization state of the clouds is directly probed by metallic line ratios and C II/C IV ratios, around 0.01 (Songaila & Cowie 1996), give typical values of the ionization parameter $U = 0.002 \rightarrow 0.03$, where $U = 4.2 \times 10^{-5} J_{21}/n$ in terms of n , the total hydrogen density, and J_{21} , the ionizing flux in units of $10^{-21} \text{ ergs cm}^{-2} \text{ s}^{-1} \text{ Hz}^{-1} \text{ sr}^{-1}$. Here we have assumed $J_\nu \sim \nu^{-\alpha}$ with $\alpha = +1.5$, following the discussion of Donahue & Shull (1991). The exact U value determined from the C II/C IV ratio depends on the details of the cloud temperature (Haehnelt *et al.* 1996), and the range of U parameters reflects this uncertainty as well as the observed range in C II/C IV ratios. For pure photoionization equilibrium $F = 3.4 \times 10^{-6} U^{-1.066}$ and the corresponding F lies in the range $1.4 \times 10^{-4} \rightarrow 2.5 \times 10^{-3}$. As Haehnelt *et al.* (1996) have emphasized, the temperature spread caused by shocking in these clouds may result in additional collisional ionization contributions, which can result in the hydrogen fraction's being substantially underestimated by photoionization equilibrium. However, the b values provide an upper limit to the temperatures of the clouds since

$$T \leq 10^4 \left(\frac{b}{13 \text{ km s}^{-1}} \right)^2 \quad (3)$$

and we can see from the distribution of b values that there are relatively few high temperature clouds in the sample. (At $z = 3$ less than 19% of the clouds can be above 10^5 K.) We have integrated the collisional ionization equilibrium though the cloud temperature distribution using the assumption that the clouds are thermally broadened to obtain a mean ratio $N(\text{H})/N(\text{H I}) = 1.6 \times 10^4$ at $z = 3$. It should be emphasized that this is an extreme upper limit, since it ignores blending and kinematic broadening contributions to the b distribution. The value is smaller at higher redshifts where the b values are lower.

We have no direct measure of the ionization parameter for the lower column density clouds, and instead must resort to indirect arguments. In the linear regime, provided reionization took place early, $T \sim n^{+0.6}$ and then in ionization equilibrium $\tau_{\text{HI}} \sim n^{+1.6}$ (Hui *et al.* 1996, Croft *et al.* 1997) which, since the b value – density distribution is also relatively invariant as a function of n_{HI} , implies $N_{\text{HI}} \sim n^{+1.6}$. The H I fraction as a function of N_{HI} column density then scales as

$$F = \frac{nT^{-0.7}}{J_{21}} \sim n^{+0.6} \sim N_{\text{HI}}^{+0.4}. \quad (4)$$

In combination with the H I power law indices of $1.38 \rightarrow 1.55$ this then implies that the contribution to Ω_b is very weakly dominated by the higher column density clouds just below the break in the DDF, whence

$$\Omega_b = \frac{H_0 \mu m_H}{c \rho_c} \int_{N_{\min}}^{N_{\text{dev}}} \frac{f_{\text{dev}}(N_{\text{HI}}/N_{\text{dev}})^{-\beta} N_{\text{HI}}}{F_{\text{dev}}(N_{\text{HI}}/N_{\text{dev}})^{0.4}} dN_{\text{HI}} \quad (5a)$$

$$= \frac{H_0 \mu m_H}{c \rho_c} \left[\frac{f_{\text{dev}} N_{\text{dev}}^2}{(1.6 - \beta) F_{\text{dev}}} \right] \left[1 - \left(\frac{N_{\min}}{N_{\text{dev}}} \right)^{1.6 - \beta} \right] \quad (5b)$$

where f_{dev} is the value of the DDF and F_{dev} the value of the neutral hydrogen at the N_{dev} column density. For $\beta = 1.45$ and $N_{\min} = 0.01 N_{\text{dev}}$ we obtain

$$\Omega_b = \left(\frac{2}{F_{\text{dev}}} \right) \Omega_b(\text{HI}) = \frac{1.2 \times 10^{-7} h^{-1}}{F_{\text{dev}}} \left(\frac{N_{\text{dev}}}{2 \times 10^{14} \text{ cm}^{-2}} \right)^{0.5} \quad (6)$$

from Table 4. Raising β to 1.55, the constant rises to 2.1, while reducing N_{\min} to 0.001 N_{dev} increases it to 2.43, and the combination would increase it to 2.7.

In order to minimize the downwards extrapolation from the metal line measurements at $N_{\text{HI}} \sim 10^{15} \text{ cm}^{-2}$ we restrict ourselves to the highest z range, where $N_{\text{dev}} \approx 10^{14.8} \text{ cm}^{-2}$ lies at the column density range probed by the metals. For $N_{\text{dev}} \approx 10^{14.8} \text{ cm}^{-2}$, where $\Omega_b(\text{HI}) = 1.2 \times 10^{-7} h^{-1}$, and $\beta = 1.53$ (Table 4), and setting $N_{\min} = 10^{11.8} \text{ cm}^{-2}$, the baryonic contribution from lower column density clouds is then

$$\Omega_b = 0.003 h^{-1} \left(\frac{F_{\text{dev}}}{10^{-4}} \right)^{-1}. \quad (7)$$

In order to obtain a conservative upper bound we assume that the C II/C IV ratios discussed above correspond to clouds with a $N(\text{H I}) \sim 10^{16} \text{ cm}^{-2}$ and adopt $U = 0.03$ at this $N(\text{H I})$. Scaling back to $10^{14.8}$ then gives F_{dev} from photoionization of 5×10^{-5} . In combination with the upper bound estimate from collisional ionization, we obtain $F_{\text{dev}} \geq 3 \times 10^{-5}$ and $\Omega_b \leq 0.01 h^{-1}$.

This is just consistent with low end estimates of the lower bound on $\Omega_b h^2$ from Weinberg *et al.* (1997), but the overlap range is surprisingly small. This discrepancy can be directly identified with the adopted limits on J by considering the overdensity at N_{dev} . From the definition of U

$$n = 2 \times 10^{-4} \left(\frac{U}{0.1} \right)^{-1} \left(\frac{J_{21}}{0.5} \right) \text{ cm}^{-3} \quad (8)$$

so that the overdensity at ionization parameter U is

$$\frac{n}{\langle n \rangle} = 26 \left(\frac{\Omega_b h^2}{0.01} \right)^{-1} \left(\frac{4.5}{1+z} \right)^3 \left(\frac{U}{0.1} \right)^{-1} \left(\frac{J_{21}}{0.5} \right). \quad (9)$$

Within the models the deviation density corresponds to an overdensity of roughly 10, and we may rewrite this as

$$J_{21} = 0.2 \left(\frac{n / \langle n \rangle}{10} \right) \left(\frac{\Omega_b h^2}{0.01} \right) \left(\frac{1+z}{4.5} \right)^3 \left(\frac{U}{0.1} \right) \quad (10)$$

so that the present results require $J_{21} < 0.2$, which then relaxes the $\Omega_b h^2$ constraints in Rauch *et al.* (1996) and Weinberg *et al.* 1997 at the expense of an inconsistency with their lower limit estimates of J .

4.4. The correlation functions

The evolution of the correlation strength with redshift is very ambiguous. As Morris *et al.* (1993) show, the distribution of the local Ly α does not follow the local galaxy distribution closely, but neither is it quite random. However, numerical simulations show that Ly α forest clouds follow the distribution of dark matter and do show the galaxy distribution more closely at $z \sim 3$ than does the observed local distribution of Ly α forest clouds. As long as the clouds are not randomly distributed, the evolution of their correlation strength with time provides a glimpse of structure formation and/or evolution in the early universe.

While the positive correlation over a small velocity range is marginally significant, another interesting feature, the anti-correlation, shows contradictory results. The existence of an anti-correlation was first claimed for spectra toward Q0055–269 (Cristiani *et al.* 1995) and

was later confirmed by Meiksin & Bouchet (1995). A similar anti-correlation is also shown in the correlation function of the Keck HIRES data at $< z > = 2.85$ (Hu *et al.* 1995). However, with a larger data set, Cristiani *et al.* (1997) claimed that there is no anti-correlation. Interestingly, the correlation function calculated at $< z > = 2.85$ for this study (only for Q0014+813 and Q0302-003) using the same Keck HIRES data does not show the anti-correlation. The results of Hu *et al.* (1995) used 4 QSOs in this redshift interval (the present two together with Q0636+680 and Q0956+120). Most of the signal in the anti-correlation arises from Q0636+680, and when this QSO is excluded the sample does not show any strong indication of the presence of an anti-correlation.

This result also gives a possible explanation for the contradictory results of Meiksin & Bouchet (1995) and Cristiani *et al.* (1997). Since Meiksin & Bouchet (1995) used only individual QSOs to look for an anti-correlation, they were able to find and confirm the early result of Cristiani *et al.* (1995). However, with the larger data set, most peculiar features in correlation functions are averaged, and no longer give the anti-correlation shown by smaller numbers of QSOs. This issue requires further work with much larger data sets.

5. Summary

We have analyzed Ly α forest clouds ($12.8 \leq \log N_{\text{HI}} \leq 16.0$) towards 5 QSOs in order to study the evolution of these clouds at $2.2 < z < 3.5$, using Keck I HIRES data. We include the Ly α forest cloud analysis at $3.4 < z < 4.0$ given by Lu *et al.* (1996) from similar quality Keck data to summarize the evolution of the Ly α forest at $2 < z < 4$.

The differential density distribution function (DDF) does not change rapidly with redshift at the lower H I column density end, being well fitted with power-laws close to ~ 1.4 . However, at the higher column density end, DDFs depart from a single power-law; at higher redshift, the amount of deviation from the power-law is smaller and the deviation column density at which DDFs start to deviate from the power-law is larger. The number density with redshift including HST observations at $z < 2$ indicates mild evolution in the number density, which reflects the behaviors of the DDFs. The minimum, mean, and median line widths of the Ly α clouds tend to increase as the redshift decreases. The correlation strength seems to increase as redshift decreases, at a velocity scale less than $\Delta v \leq 300 \text{ km s}^{-1}$. The fluctuation power spectrum at near-Mpc scales (*c.f.*, Hui *et al.* 1996) is found to be 1.15 ± 0.1 , while the contribution to Ω_b from forest clouds ($12.8 < \log N_{\text{HI}} < 14.8$) at $z = 3.5$ is $\Omega_b \lesssim 0.01 h^{-1}$.

REFERENCES

Bahcall, J. N., *et al.* 1993, ApJS, 87, 1.

Bajtlik, S., Duncan, R. C., & Ostriker, J. P. 1988, ApJ, 327, 570.

Bechtold, J. 1994, ApJS, 91, 1

Bi, H. & Davidsen, A. F. 1997, ApJ, 479, 528 [astro-ph/9611062]

Boksenberg, A. 1995, in QSO Absorption Lines, edited by G. Meylan (Springer, Berlin), p. 253

Cen, R., Miralda-Escudé, J., Ostriker, J. P., & Rauch, M. 1994, ApJ, 437, L9

Cooke, A., Espey, B., & Carswell, B. 1997, MNRAS, 284, 552 [astro-ph/9609100]

Cowie, L. L., Songaila, A., Kim, T.-S., & Hu, E. M. 1995, AJ, 109, 1522

Cristiani, S., D’Odorico, S., Fontana, A., Giallongo, E., & Savaglio, S. 1995, MNRAS, 273, 1016

Cristiani, S., D’Odorico, S., D’Odorico, V., Fontana, A., Giallongo, E., & Savaglio, S. 1997, MNRAS, 285, 209 [astro-ph/9610006]

Croft, R. A. C., Weinberg, D. H., Hernquist, L., & Katz, N. 1997, to appear in Proceedings of the 18th Texas Symposium on Relativistic Astrophysics, edited by A. Olinto, J. Friedman, and D. Schramm (World Scientific: Singapore) [astro-ph/9701166]

Davé, R., Hernquist, L., Weinberg, D. H., & Katz, N. 1997, ApJ, 477, 21 [astro-ph/9609115]

Donahue, M., & Shull, J. M. 1991, ApJ, 383, 511

Ferland, G. J. 1993, Univ. of Kentucky Department of Physics and Astronomy Internal Report, (Cloudy C84)

Giallongo, E., & Petitjean, P. 1994, ApJ, 426, L61

Haehnelt, M. G., Rauch, M., & Steinmetz, M. 1996, MNRAS, 283, 1055 [astro-ph/9608133]

Haardt, F., & Madau, P. 1996, ApJ, 461, 20 [astro-ph/9509093]

Hernquist, L., Katz, N., Weinberg, D. H., & Miralda-Escudé, J. 1996, ApJ, 457, L51

Hogan, C. J., Anderson, S. F., & Rugers, M. H. 1997, AJ, in press [astro-ph/9609136]

Hu, E. M., Kim, T.-S., Cowie, L. L., Songaila, A., & Rauch, M. 1995, AJ, 110, 1526

Hui, L., & Gnedin, N. Y. 1996, MNRAS, submitted [astro-ph/9612232]

Hui, L., Gnedin, N. Y., & Zhang, Y. 1996, ApJ, submitted [astro-ph/9608157]

Impey, C. D., Petry, C. E., Malkan, M. A., & Webb, W. 1996, ApJ, 463, 473

Kirkman, D., & Tytler, D. 1997, AJ, in press [astro-ph/9701209]

Lanzetta, K. M., Wolfe, A. M., Turnshek, D. A., Lu, L., McMahon, R. G., & Hazard, C. 1991, ApJS, 77, 1

Lu, L., Sargent, W. L. W., Womble, D. S., & Takada-Hidai, M. 1996, ApJ, 472, 509

Lu, L., Wolfe, A. M., & Turnshek, D. A. 1991, ApJ, 367, 19

Meiksin, A., & Bouchet, F. R. 1995, ApJ, 448, L85

Morris, S. L., Weymann, R. J., Dressler, A., McCarthy, P. J., Smith, B. A., Terrile, R. J., Giovanelli, R., & Irwin, M. 1993, ApJ, 419, 524

Mücket, J. P., Petitjean, P., Kates, R. E., & Riediger, R. 1996, A&A, 308, 17

Mücket, J. P., Petitjean, P., & Riediger, R. 1997, A&A, submitted

Murdoch, H. S., Hunstead, R. W., Pettini, M., & Blades, J. C. 1986, ApJ, 309, 19

Petitjean, P., Webb, J. K., Rauch, M., Carswell, R. F., & Lanzetta, K. M. 1993, MNRAS, 262, 499

Rauch, M., Carswell, R. F., Chaffee, F. H., Foltz, C. B., Webb, J. K., Weymann, R. J., Bechtold, J., & Green, R. F. 1992, ApJ, 390, 387

Rauch, M., Miralda-Escudé, J., Sargent, W. L. W., Barlow, T. A., Weinberg, D. H., Hernquist, L., Katz, N., Cen, R., & Ostriker, J. P. 1996, ApJ, submitted [astro-ph/9612245]

Reimers, D., & Vogel, S. 1993, A&A, 276, L13

Rodriguez-Pascual, P. M., de la Fuente, A., Sanz, J. L., Recondo, M. C., Clavel, J., Santos-Lleo, M., & Wamsteker, W. 1995, ApJ, 448, 575

Sargent, W. L. W., Young, P. J., Boksenberg A., & Tytler D. 1980, ApJS, 42, 41

Songaila, A. 1997, in preparation

Songaila, A., & Cowie, L. L. 1996, AJ, 112, 335

Véron-Cetty, M.-P., & Véron, P. 1996, A Catalogue of Quasars and Active Nuclei, 7th ed., *ESO Scientific Report No. 17*

Vogel, S., & Reimers, D. 1995, A&A, 294, 377

Weinberg, D. H., Miralda-Escudé, J., Hernquist, L., & Katz, N. 1997, ApJ, submitted [astro-ph/9701012]

Zhang, Y., Anninos, P., & Norman, M. L. 1995, ApJ, 453, L57

Zhang, Y., Anninos, P., Norman, M. L., & Meiksin, A. 1997, ApJ, in press [astro-ph/9609194]

Table 1. Fitted QSOs

QSO	V	z_{em}	t_{exp}	λ_{range} (Å)	$z_{\text{Ly}\alpha}$	dX^a	# of lines
Q1623+268	16.0	2.521	5 ^h 20 ^m	3850 – 4195	2.17 – 2.45	0.939	68 ^b
Q1700+643	16.1	2.722	2 40	3850 – 4195	2.17 – 2.45	0.939	82
Q0014+813	16.5	3.387	8 15	4510 – 4863	2.71 – 3.00	1.023	118
Q0302–003	17.6	3.290	10 00	4510 – 4863	2.71 – 3.00	1.119	123
Q1422+231	16.5 ^c	3.620	9 40	5105 – 5485	3.20 – 3.51	1.233	146

Note. — Magnitudes and redshifts are taken from Véron-Cetty & Véron (1996).

^aThe redshift path is defined as $X \equiv 0.5[(1+z)^2 - 1]$, for $q_0 = 0$.

^bThe number of lines is for $N_{\text{HI}} = 10^{13.1} - 10^{14.3} \text{ cm}^{-2}$.

^cR magnitude.

Table 2. Incompleteness correction^a

$\log N_{\text{HI}}$	$< z > = 2.31$		$< z > = 3.35$	
	Incompleteness	$\log f$	Incompleteness	$\log f$
12.8 – 13.1	0.68	–11.37	0.44	–11.02
13.1 – 13.4	1.00	–11.68	0.72	–11.54
13.4 – 13.7	0.92	–12.04	0.78	–11.93
13.7 – 14.0	0.89	–12.58	0.89	–12.53
14.0 – 14.3	0.90	–12.94	0.91	–12.90

^aFor the incompleteness correction for the $< z > = 2.85$ forest clouds, the results of Hu *et al.* (1995) were used.

Table 3. Median b values of the observed QSOs

QSO	$N_{\text{HI}} = 10^{13.8} - 10^{16} \text{ cm}^{-2}$ (km s $^{-1}$)	$N_{\text{HI}} = 10^{13.1} - 10^{14} \text{ cm}^{-2}$ (km s $^{-1}$)
Q1623+268	41	36
Q1700+643	35	28
Q0014+813	34	31
Q0302–003	37	29
Q1422+231	30	27
Q0000-003 ^a	31	29

Note. — Median b values over the indicated column density ranges.

^aFrom Lu *et al.* 1996

Table 4. Ω_b of neutral hydrogen

Parameters	$< z > = 2.31$	$< z > = 2.85$	$< z > = 3.35$	$< z > = 3.70$
$N_{\text{HI,dev}} \text{ (cm}^{-2}\text{)}$	$10^{14.3}$	$10^{14.3}$	$10^{14.8}$	—
$f(N_{\text{HI}})$	$1.5 \times 10^6 N_{\text{HI}}^{-1.35}$	$4.9 \times 10^7 N_{\text{HI}}^{-1.46}$	$4.5 \times 10^8 N_{\text{HI}}^{-1.53}$	$9.5 \times 10^8 N_{\text{HI}}^{-1.55}$
$\Omega_b(\log N_{\text{HI}} < 14.3)$	5.7×10^{-8}	6.0×10^{-8}	6.3×10^{-8}	7.2×10^{-8}
$\Omega_b(\log N_{\text{HI}} < 15.5)$	1.1×10^{-7}	1.3×10^{-7}	2.1×10^{-7}	2.5×10^{-7}

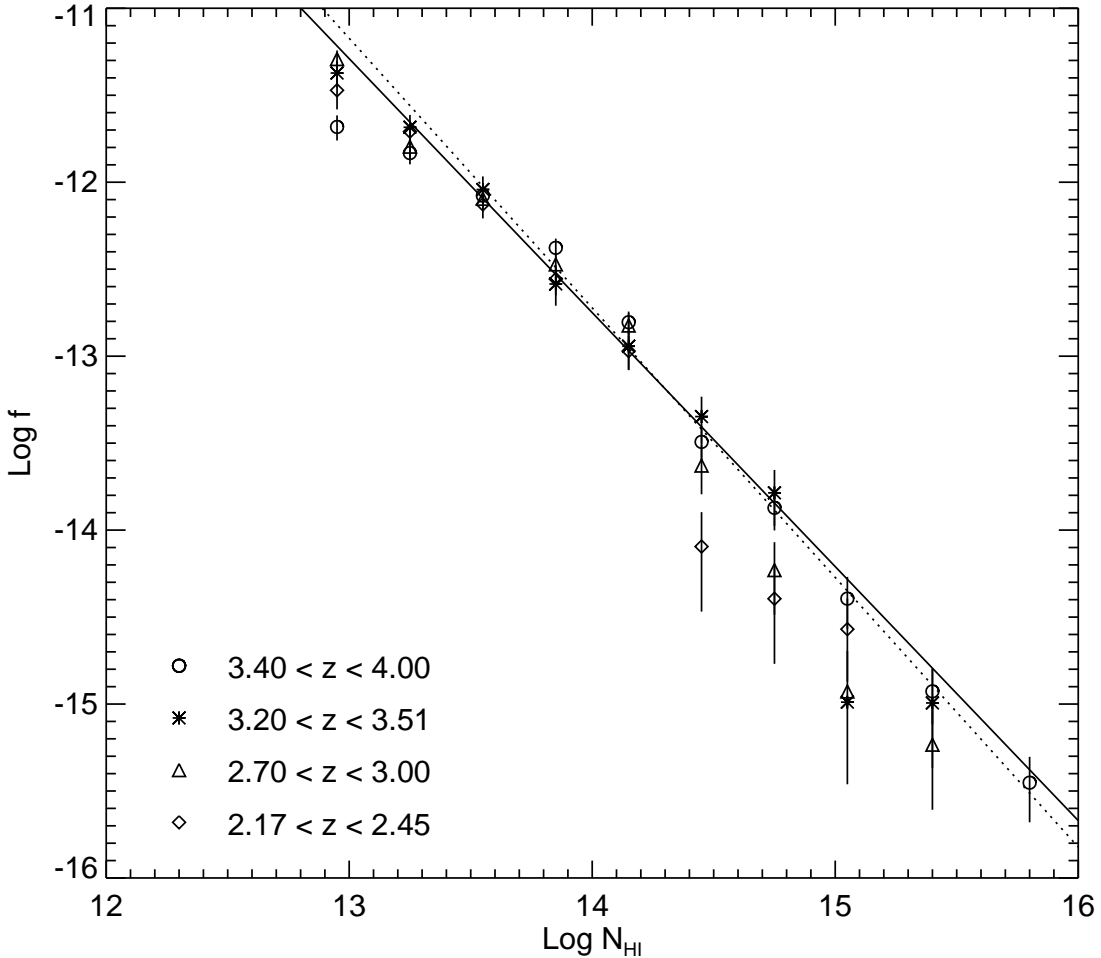


Fig. 1.— Differential density distribution function without incompleteness correction. The distribution with H I column density is shown for each of three indicated redshift bins, with 1σ error bars, compared with the results of Lu *et al.* (1996) (open circles). The solid line represents the single power-law fit, $f(N_{\text{HI}}) = 4.9 \times 10^7 N_{\text{HI}}^{-1.46}$. The dotted line shows the single power-law fit taken from Lu *et al.* (1996) for $< z >= 3.7$, which is $f(N_{\text{HI}}) \propto N_{\text{HI}}^{-1.55}$ for $12.6 < \log N_{\text{HI}} < 16.0$. At $N_{\text{HI}} \leq 10^{14} \text{ cm}^{-2}$, the distribution functions at different redshifts look very similar, and lack significant flattening. However, at $N_{\text{HI}} \geq 10^{14} \text{ cm}^{-2}$, the amount of deficiency in forest clouds compared to the expected power-law distribution depends on redshift. The deviation from the power law moves to smaller N_{HI} as redshift decreases, which means the higher N_{HI} forest clouds evolve rapidly.

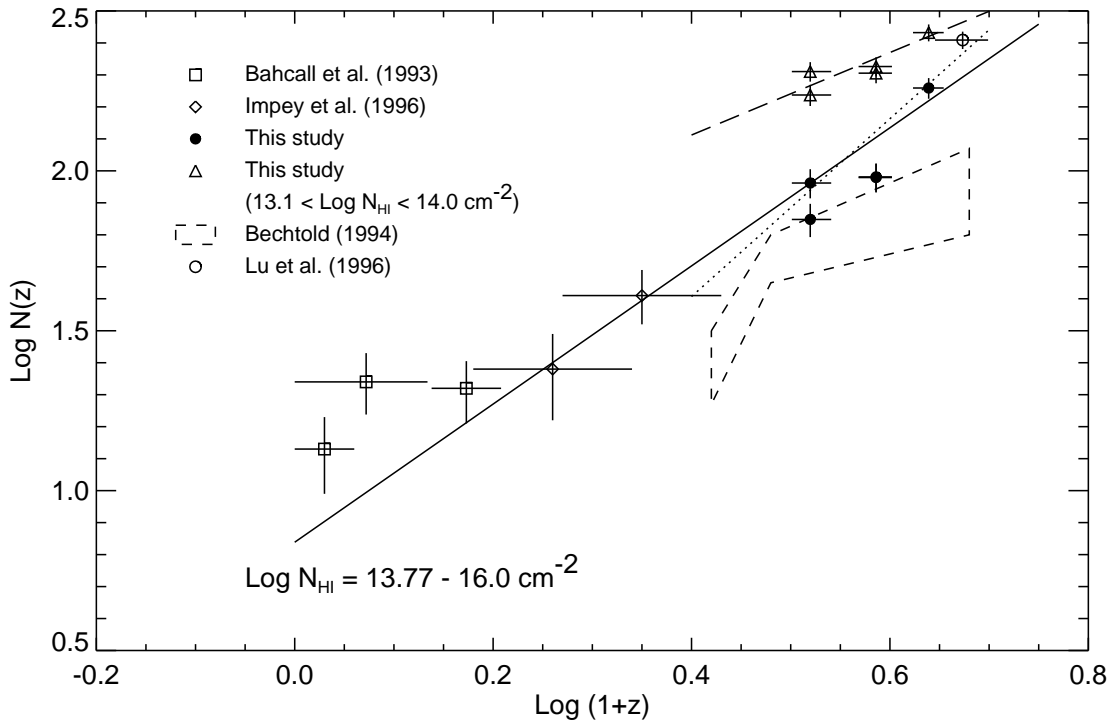


Fig. 2.— $N(z)$ vs redshift for the present data (filled circles) and the HST observations (open squares and open diamonds). The region outlined with dashed lines shows the results from Bechtold (1994). The solid line shows the maximum likelihood fit to the HST data and the high column density Keck data (slope $\gamma = 2.15$). The dotted line shows the fit to the Keck data only, with a slope of $\gamma = 2.78$. Triangles show the forest clouds over just the column density range $N_{\text{HI}} = 10^{13.1} - 10^{14} \text{ cm}^{-2}$, with a long dashed line fit with $\gamma = 1.19$. The 1σ error bars and redshift binning are indicated for each point.

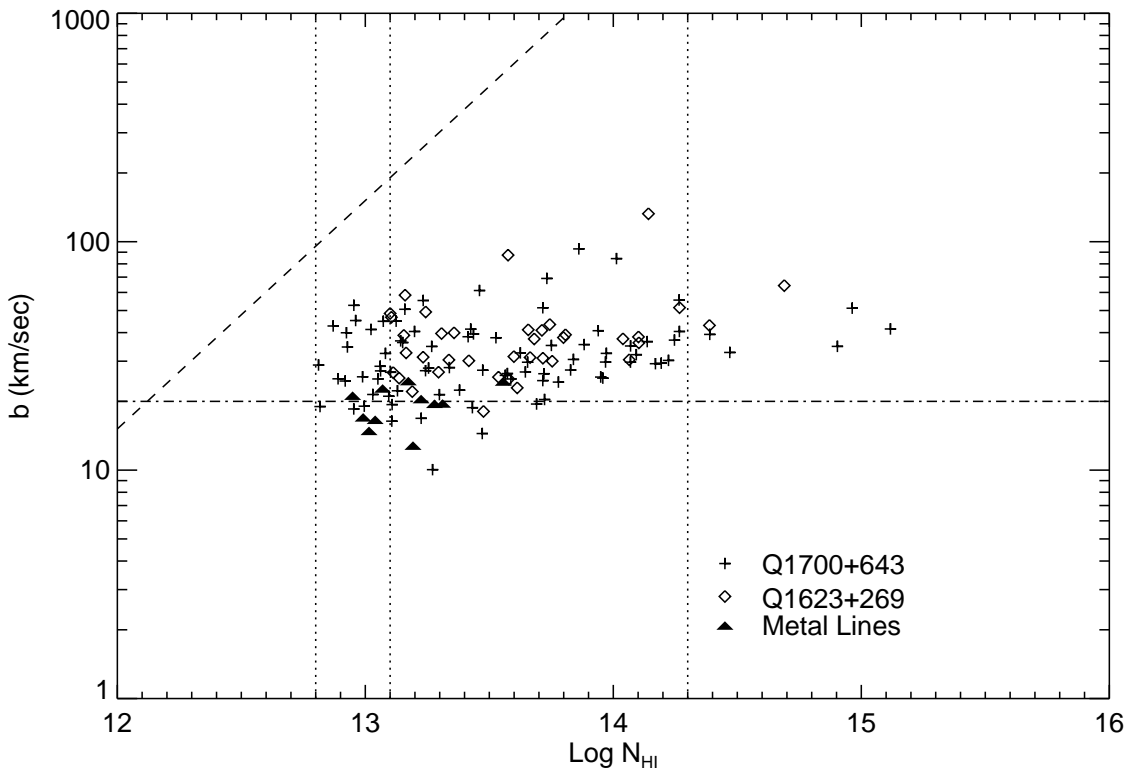


Fig. 3a.— $b - \log N_{\text{HI}}$ diagram at $< z > = 2.17 - 2.45$. The dot-dashed line shows $b = 20 \text{ km s}^{-1}$. Note that there are not many lines with $N_{\text{HI}} \geq 10^{14} \text{ cm}^{-2}$. The vertical dotted lines show the adopted minimum N_{HI} and the value at which the clouds saturate, while the dashed line shows the optical depth selection limit.

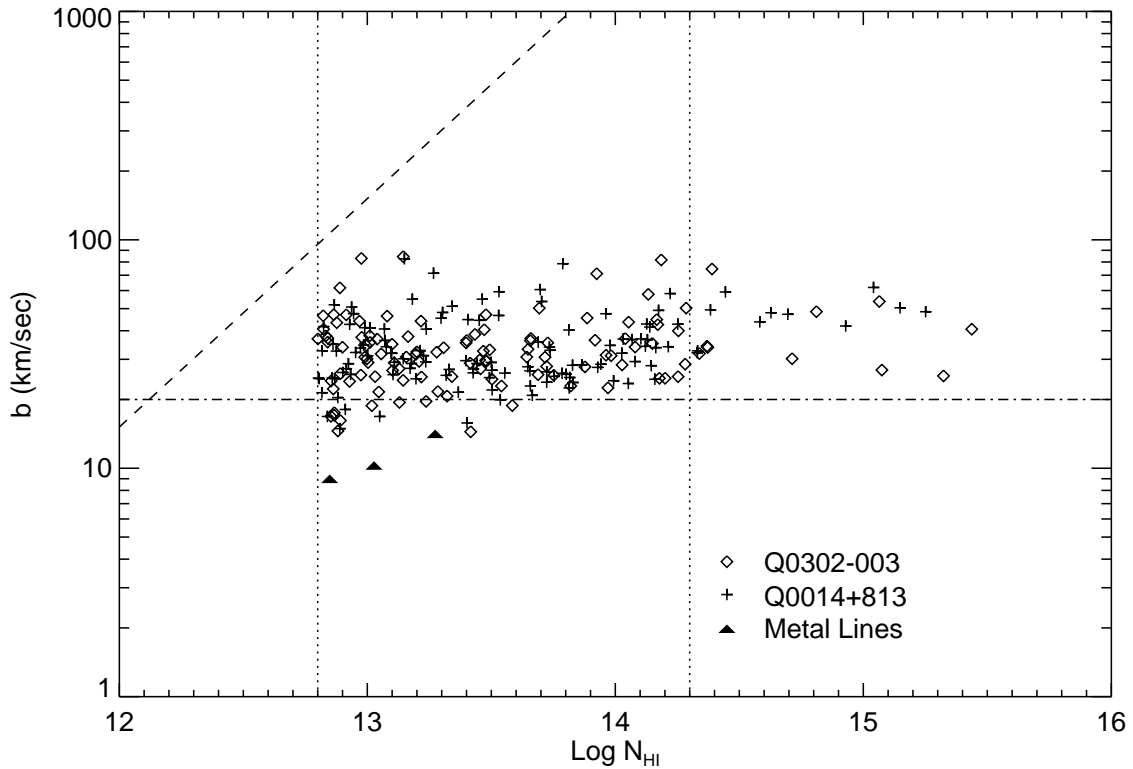


Fig. 3b.— $b - \log N_{\text{HI}}$ diagram at $< z > = 2.70 - 3.00$. The dot-dashed line shows $b = 20 \text{ km s}^{-1}$. Note that there are many more lines with $N_{\text{HI}} \geq 10^{14} \text{ cm}^{-2}$ compared to the same range in column density for $z = 2.17 - 2.45$.

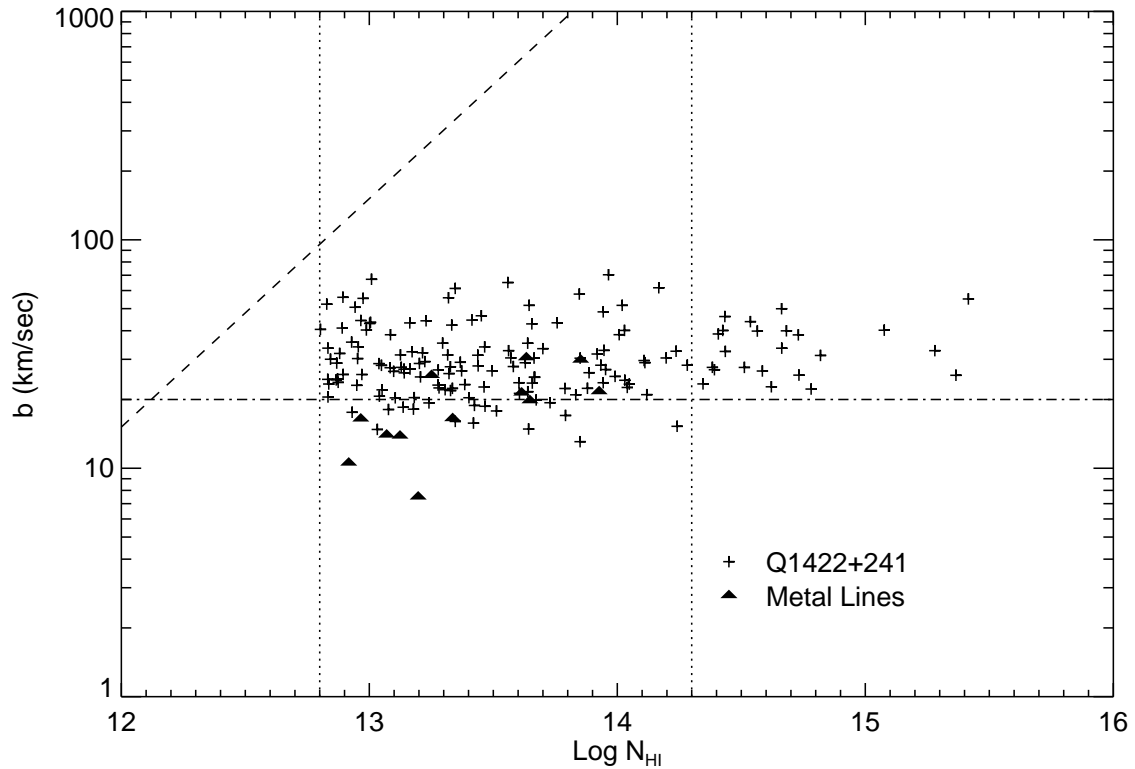


Fig. 3c.— $b - \log N_{\text{HI}}$ diagram at $\langle z \rangle = 3.20 - 3.51$. The dot-dashed line shows $b = 20 \text{ km s}^{-1}$. Note the increase in the number of lines with $b < 20 \text{ km s}^{-1}$ over this redshift range compared to $\langle z \rangle = 2.31$ and $\langle z \rangle = 2.85$.

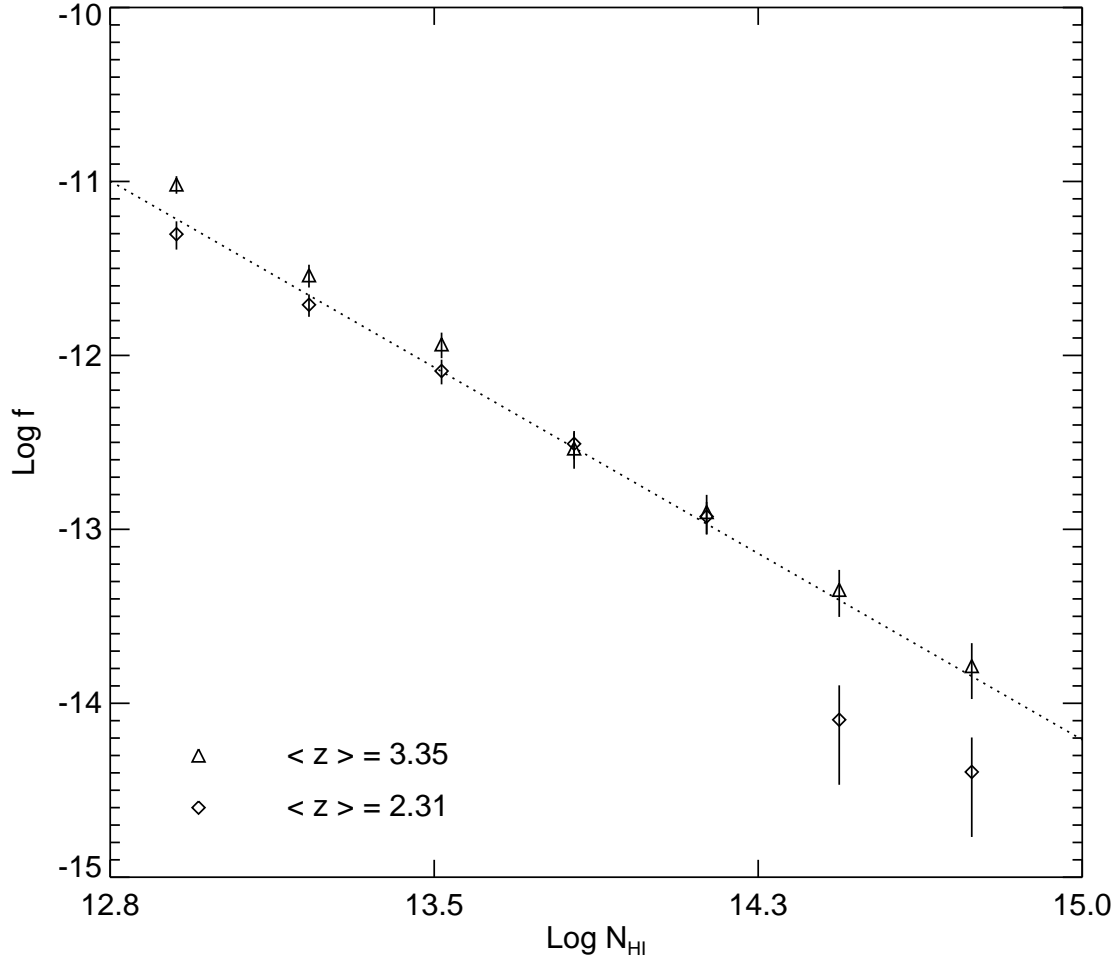


Fig. 4a.— Incompleteness corrected differential density distribution functions with redshift. Diamonds are $< z > = 2.31$ clouds and triangles are $< z > = 3.35$ systems. 1σ error bars are shown for each point. The dotted line is the same power-law fit shown in Fig. 1. See the discussion in Sec. 3.3 for more details.

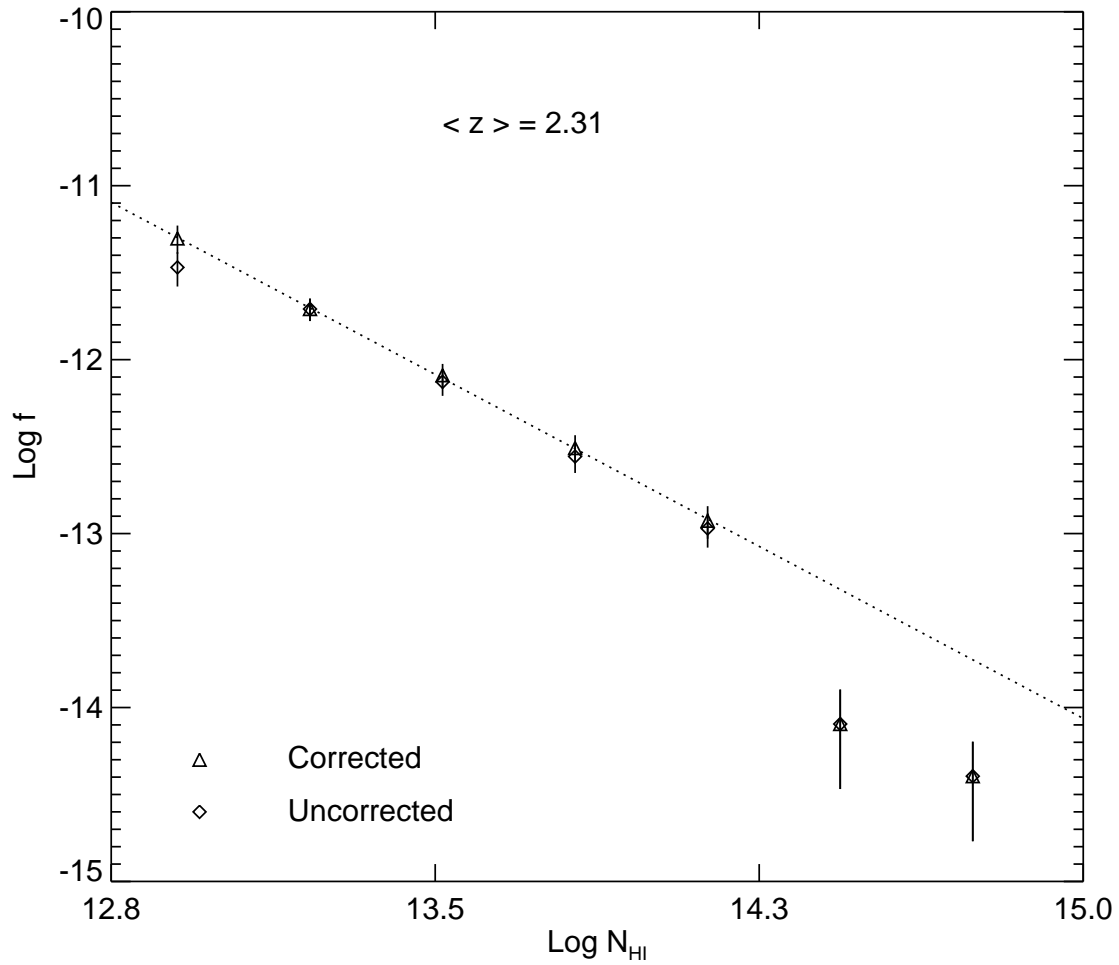


Fig. 4b.— Corrected and uncorrected differential density distribution functions at $\langle z \rangle = 2.31$. The deviation from the power-law fit at column densities above $N_{\text{HI}} = 2 \times 10^{14} \text{ cm}^{-2}$ may be clearly seen.

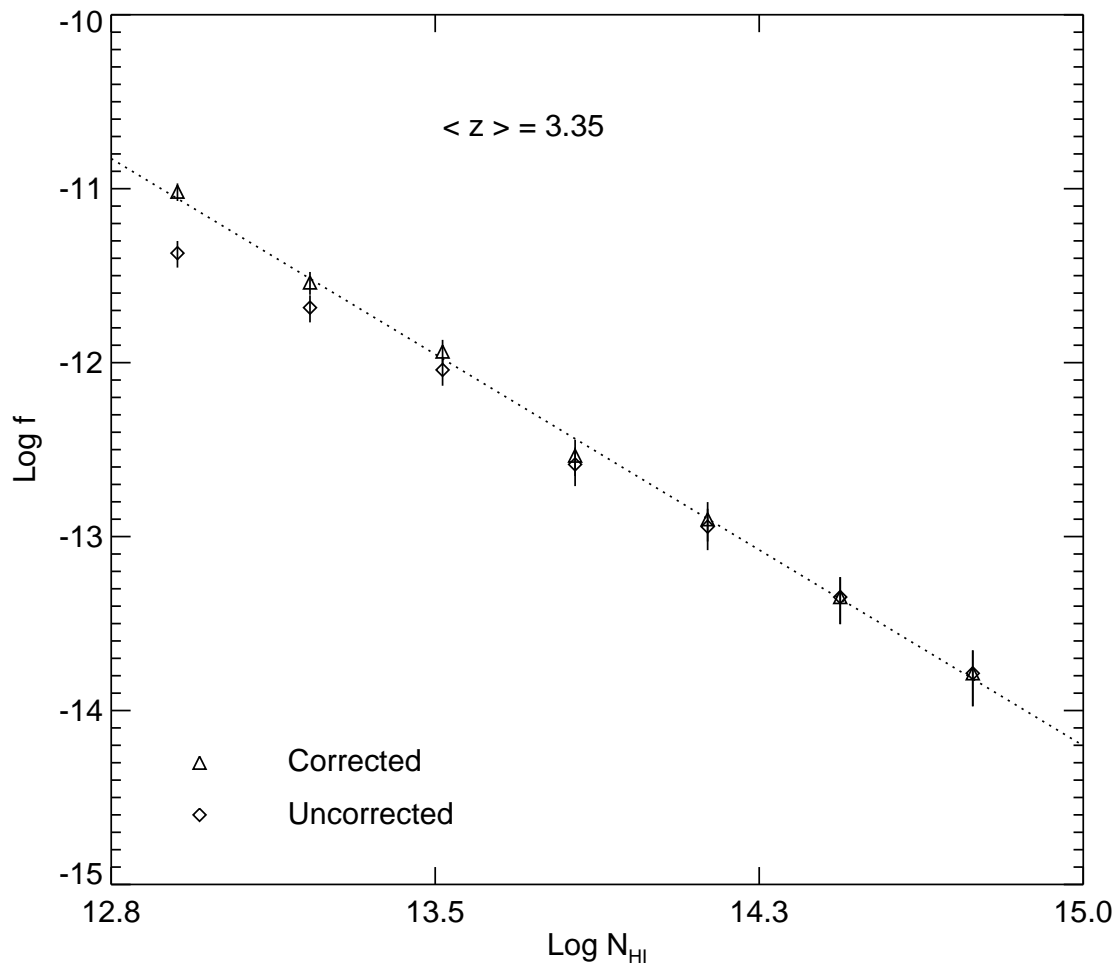


Fig. 4c.— Corrected and uncorrected differential density distribution functions at $< z > = 3.35$.

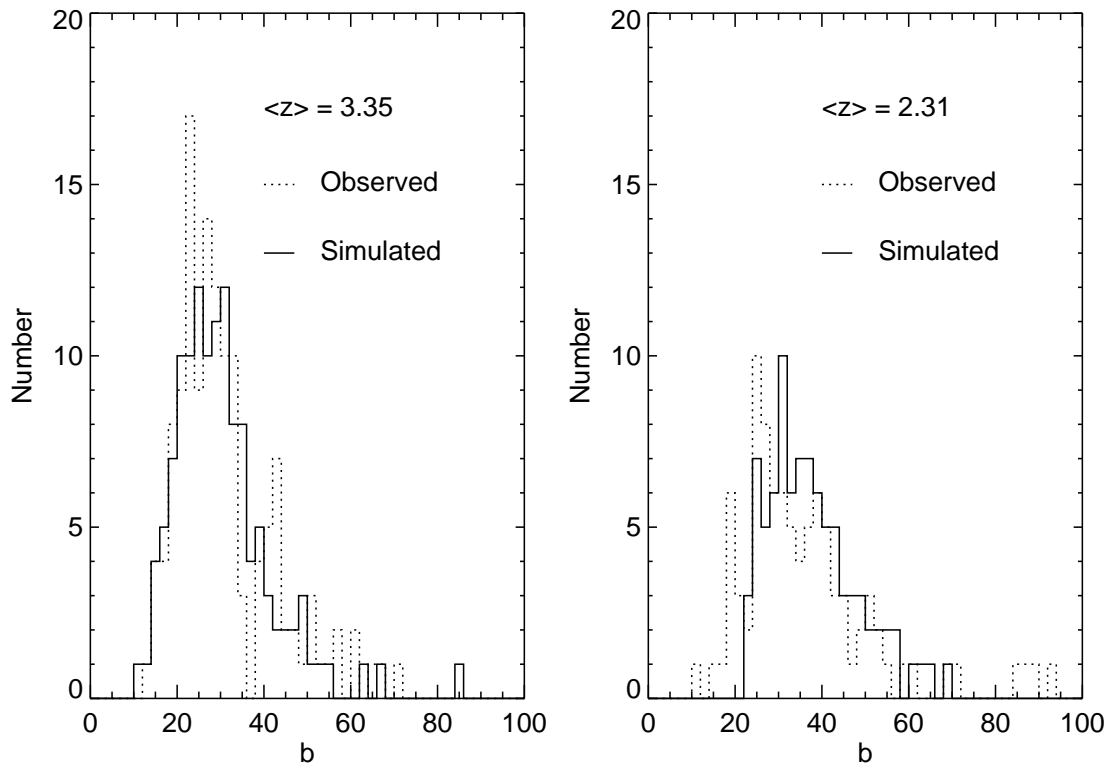


Fig. 5.— Observed (dotted histogram) and simulated (solid histogram) b distributions. For the $\langle z \rangle = 3.35$ clouds, the low cut-off b value is $\sim 17 \text{ km s}^{-1}$. For the $\langle z \rangle = 2.31$ clouds, there is no single best-fit assumed distribution for b . Assuming that most narrow lines are unidentified metal lines towards Q1700+643 and ignoring the lines with $b < 22 \text{ km s}^{-1}$, the cut-off b of 24 km s^{-1} which is shown in the figure best fits the data.

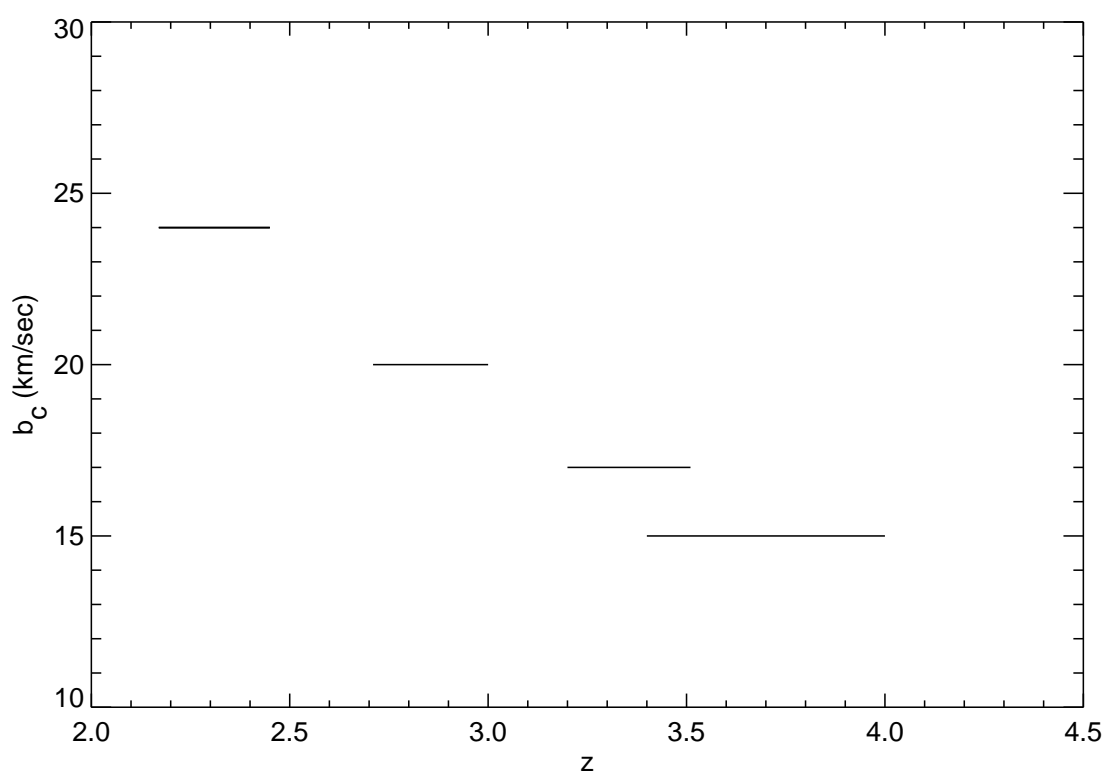


Fig. 6a.— Evolution of b_c with redshift.

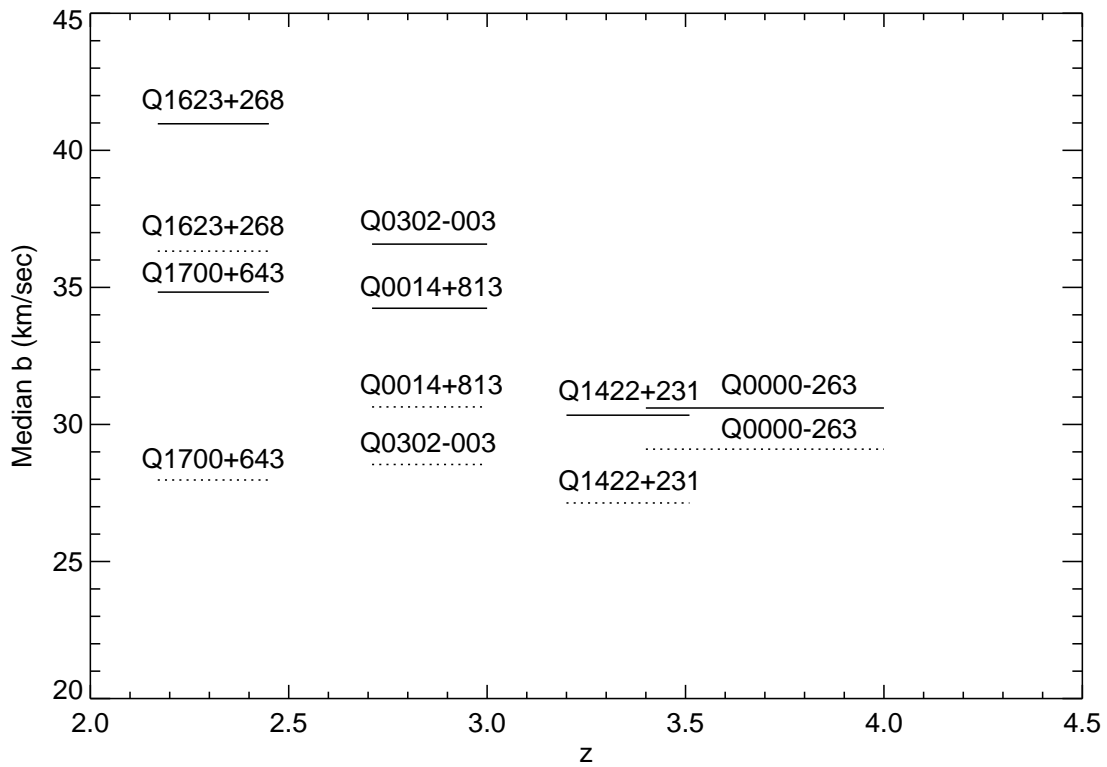


Fig. 6b.— Evolution of median b values with redshift. The solid line is for $N_{\text{HI}} = 10^{13.8} - 10^{16} \text{ cm}^{-2}$, and the dotted line is for $N_{\text{HI}} = 10^{13.1} - 10^{14} \text{ cm}^{-2}$. There is a general trend of increasing b values as redshift decreases for both column density selections, though the effect is more pronounced in the higher column density systems.

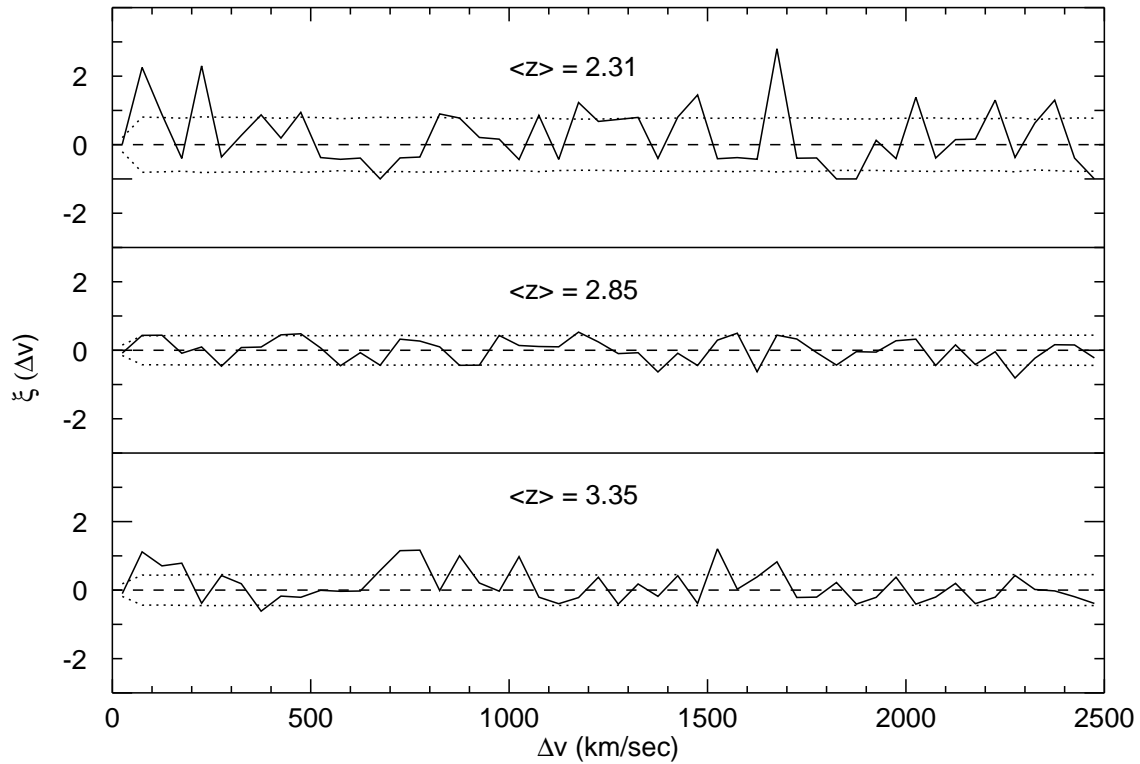


Fig. 7a.— The redshift-averaged correlation functions. The dotted lines show the 1σ Poisson uncertainty. At $\langle z \rangle = 2.31$ and $\langle z \rangle = 3.35$, there is a positive correlation at $\Delta v < 300 \text{ km s}^{-1}$.

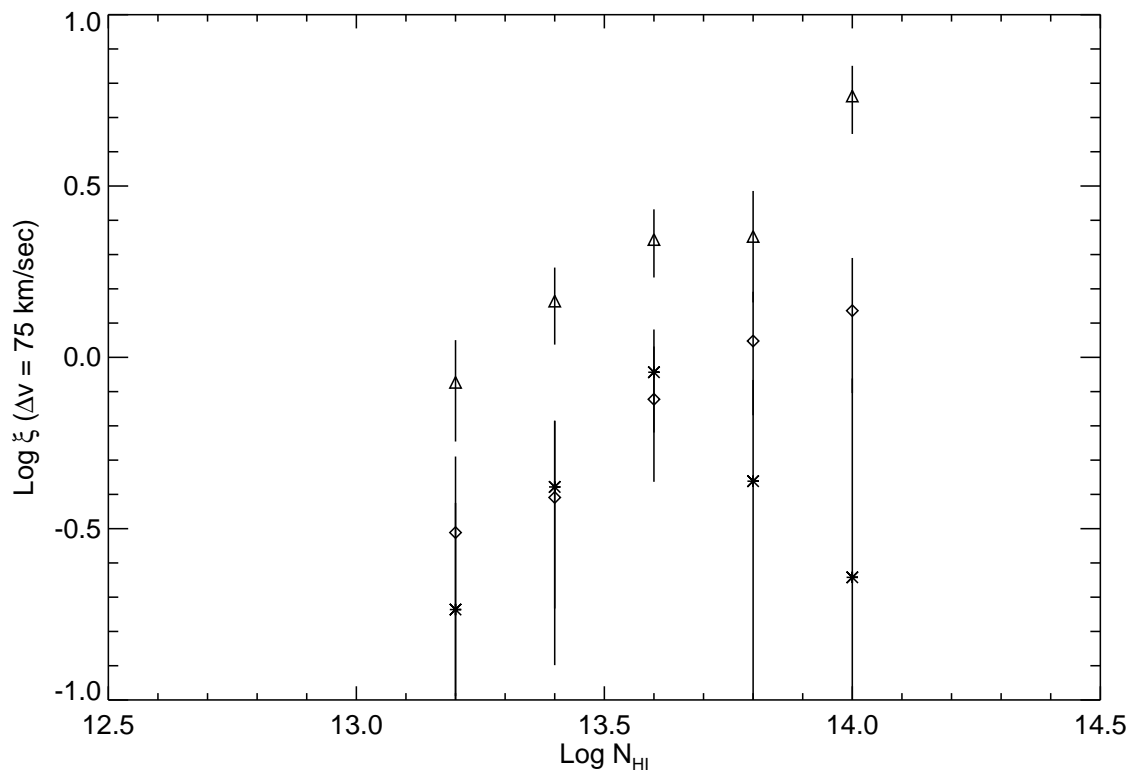


Fig. 7b.— The correlation strengths at $\Delta v = 75 \text{ km s}^{-1}$ with $N_{\text{HI,th}}$ at different redshifts.

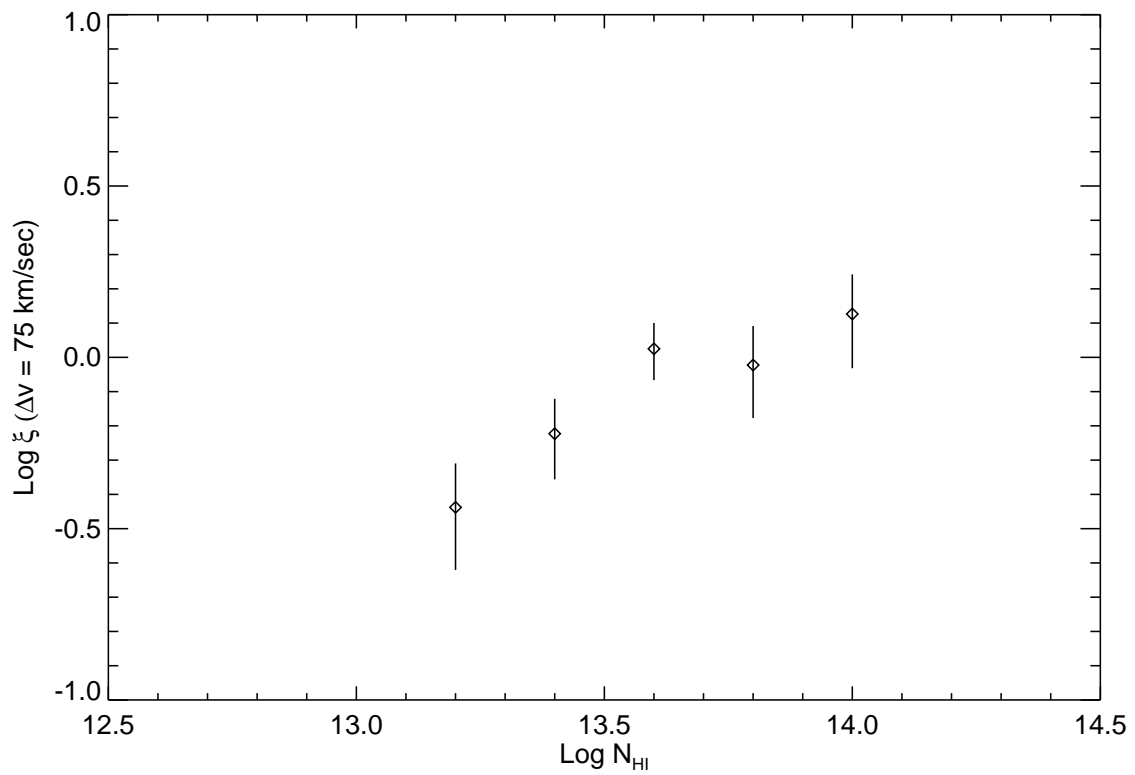


Fig. 7c.— The redshift-averaged correlation strengths at $\Delta v = 75 \text{ km s}^{-1}$ with $N_{\text{HI,th}}$.

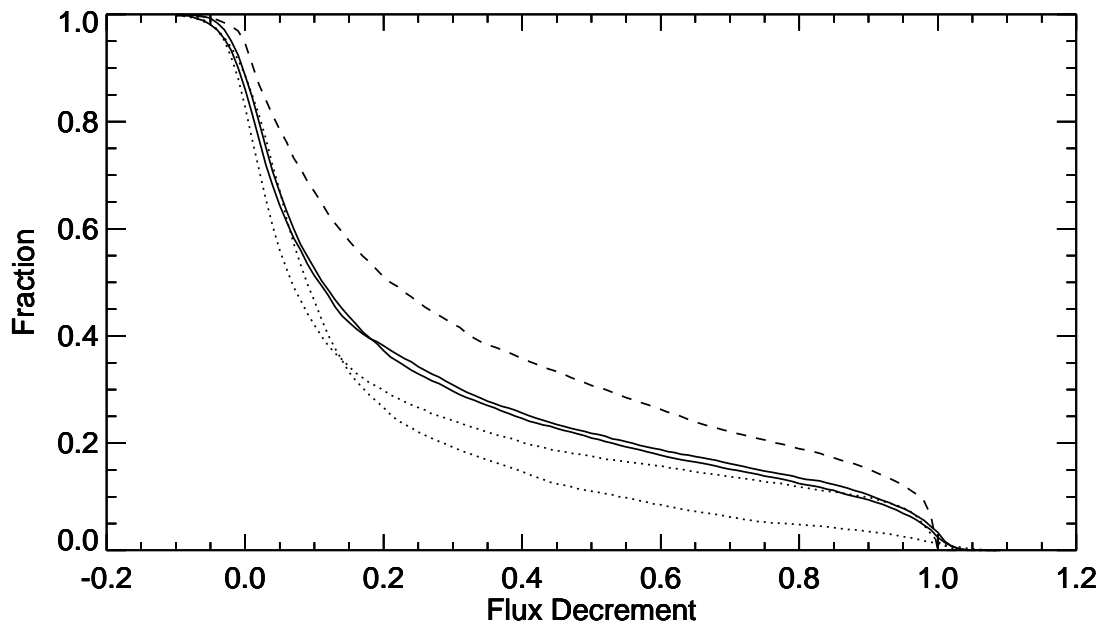


Fig. 8a.— Normalized cumulative distribution of flux decrements for the 5 quasars. The dashed line shows the $\langle z \rangle = 3.35$ system, the solid lines the $\langle z \rangle = 2.85$ systems, and the dotted lines the $\langle z \rangle = 2.31$ systems.

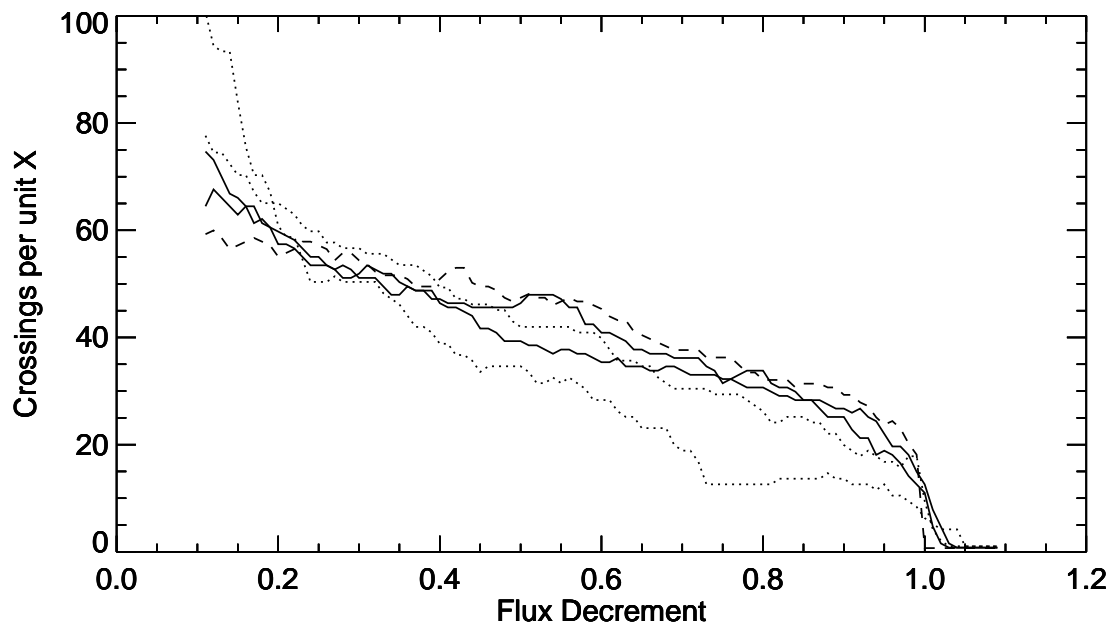


Fig. 8b.— Number of down-crossings per unit X plotted vs. flux decrement. Redshift identifications as for part a).

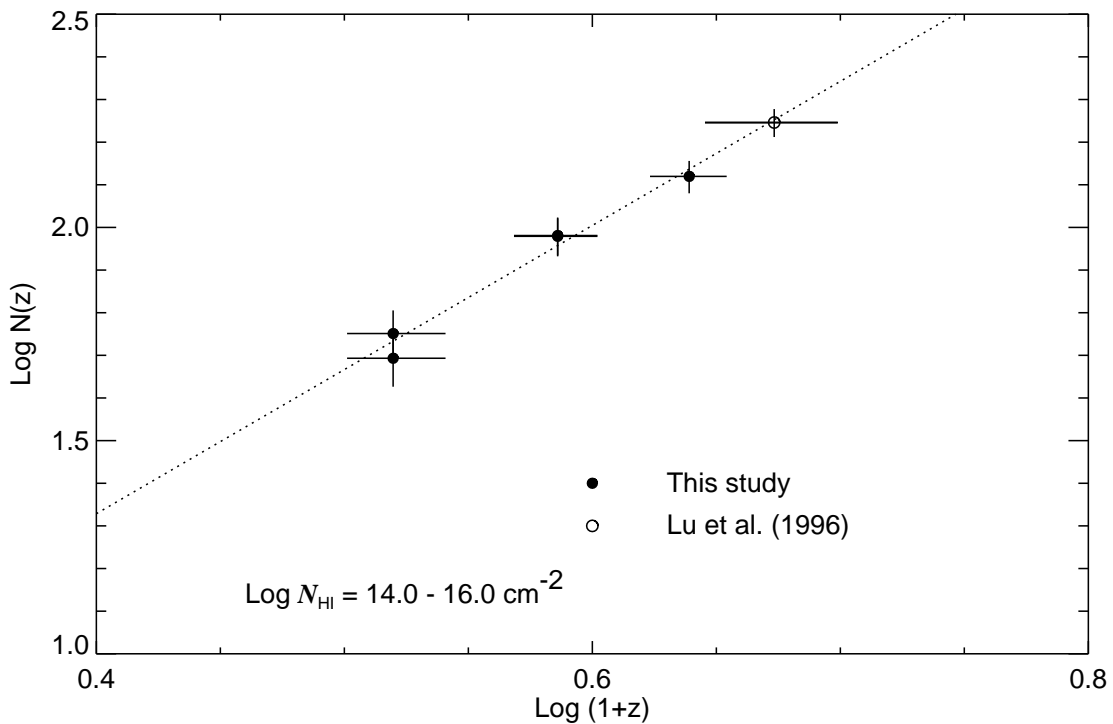


Fig. 9.— $N(z)$ vs redshift at $N_{\text{HI}} = 10^{14-16} \text{ cm}^{-2}$. The filled circles show our data points, while the open circle is taken from Lu *et al.* (1996). For Q0014+813 and Q0302-003, the $N(z)$ values are nearly identical, and are marked with a single overlapping data point. The data show a uniform trend with a steep rise in the number density evolution. The dotted line shows a least-squares fit to $N(z) \propto (1 + z)^{3.38}$.

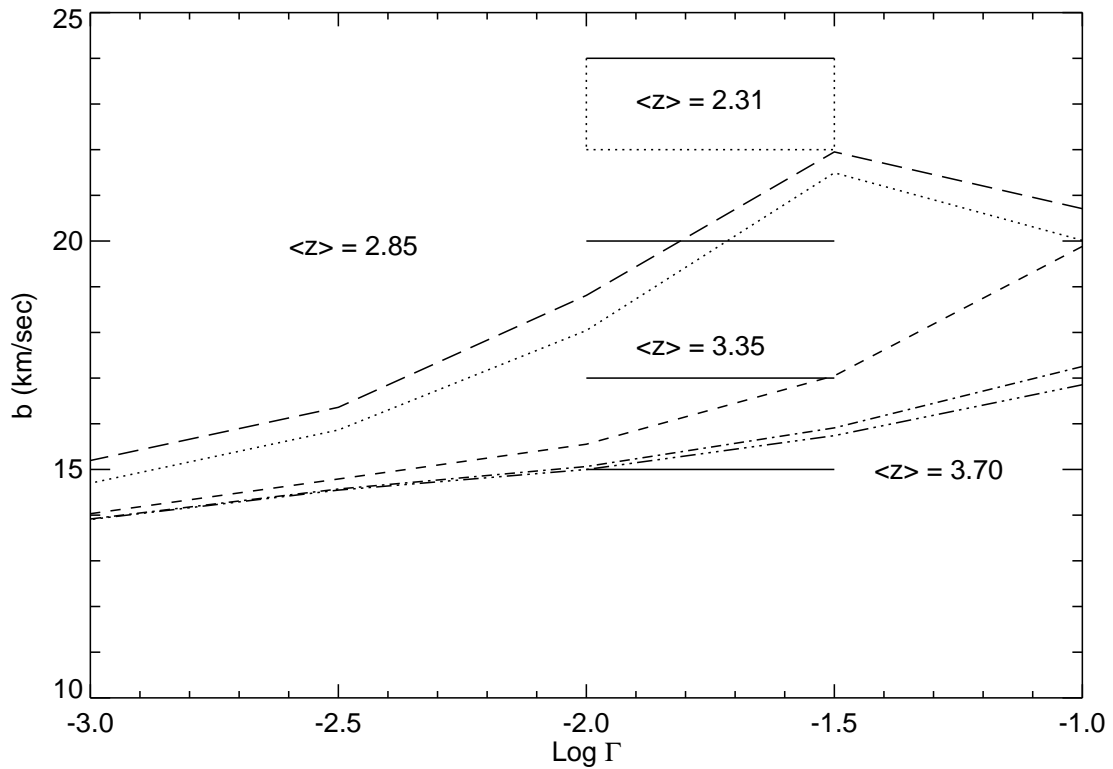


Fig. 10.— Photoionization and b values. The lines were calculated from the photoionization model for the assumed He II ionization at $z \sim 3.1$. See the discussion in Sec. 4.2 for more details.